iScience

CellPress
OPEN ACCESS

Article

JLP/Foxk1/N-cadherin axis fosters a partial epithelial-mesenchymal transition state in epithelial tubular cells

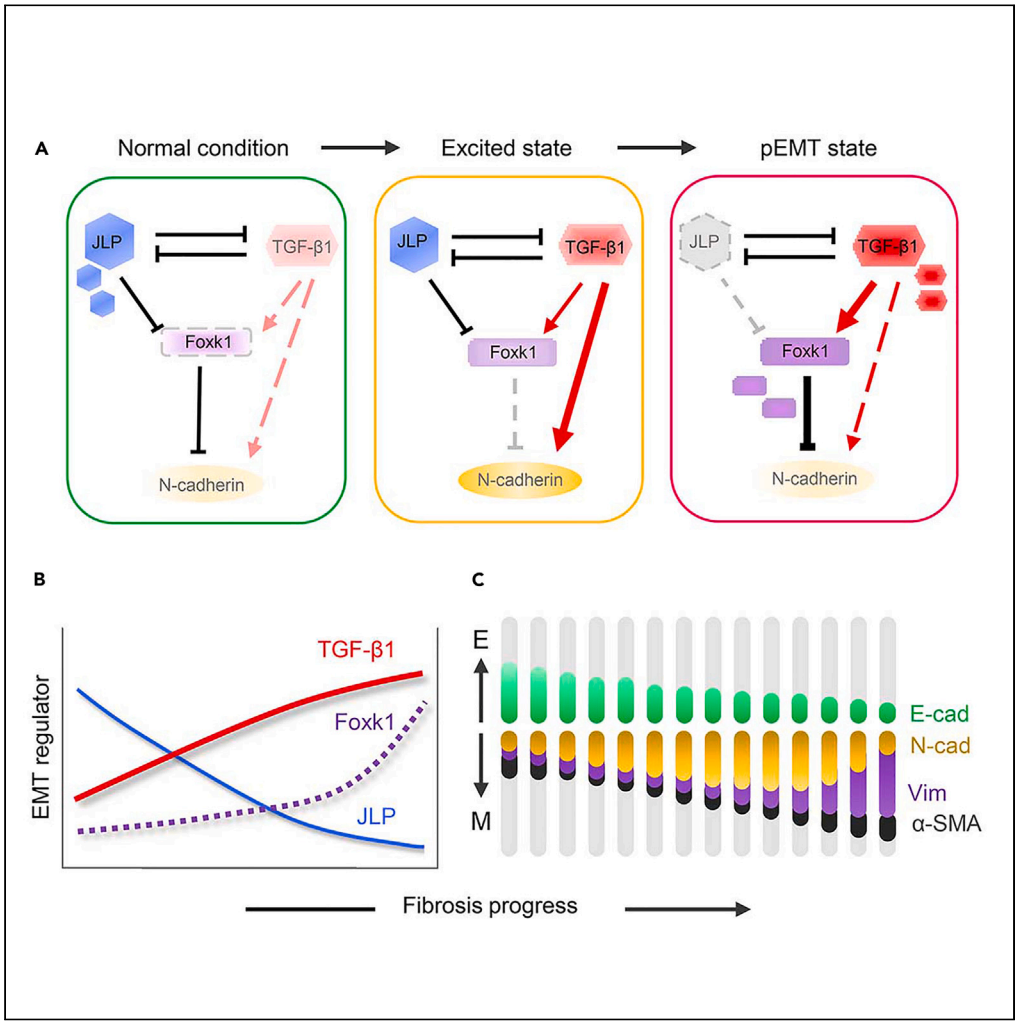

Maoqing Tian, Lu Zhang, Meng Zhang, ..., Zhongping Wei, Yujuan Wang, Huiming Wang

rm000301@whu.edu.cn

Highlights

Phenotypic alteration of TECs is crucial in limiting the process of kidney fibrosis

N-cadherin is a functional and phenotypic landmark of pEMT

Loss of N-cadherin in tubular cells aggravates renal fibrosis

JLP/Foxk1/N-cadherin axis regulates renal fibrosis progression

Tian et al., iScience 26, 106396
April 21, 2023
https://doi.org/10.1016/j.isci.2023.106396

iScience

CellPress
OPEN ACCESS

Article

JLP/Foxk1/N-cadherin axis fosters a partial epithelial-mesenchymal transition state in epithelial tubular cells

Maoqing Tian,[1,3] Lu Zhang,[1,3] Meng Zhang,[1,3] Liwen Qiao,[1] Bingqing Xu,[1] Chen Li,[1] Shan Liu,[1,2] Yuan Song,[1] Zhongping Wei,[1] Yujuan Wang,[1] and Huiming Wang[1,4,*]

SUMMARY

Renal tubular epithelial cells (TECs) undergoing partial epithelial-mesenchymal transition (pEMT) during renal fibrosis has been recognized as a featuring and detrimental event. However, the mechanism for redirecting the cell fate of pEMT remains unclear. Here we mapped the temporal expression trajectories of a series of EMT-related molecules in renal fibrosis. It revealed a unique expression profile of N-cadherin of initial rising and late dropdown, which is distinct from that of other mesenchymal markers. The transcription factor Foxk1, which serves as a negative regulator of the N-cadherin gene, was induced by TGF-β1 but was tightly regulated in the presence of JNK-associated leucine zipper protein (JLP). The loss of JLP resulted in Foxk1 induction, leading to N-cadherin downregulation and compromised cell viability. We propose a novel axis consisting of JLP/Foxk1/N-cadherin in shaping the EMT program and suggest JLP as the checkpoint of the EMT continuum during renal fibrosis progression.

INTRODUCTION

Epithelial-to-mesenchymal transition (EMT) is a process of cell phenotypic conversion from epithelial to mesenchymal, in which epithelial cells lose their junctions and polarity to gain a motile trait.[1] EMT is an essential physiological process in embryogenesis and wound healing; however, its aberrant activation is also involved in pathological conditions such as fibrosis and cancer.[2] Kidney interstitial fibrosis is a common pathological outcome of uncontrolled tissue injury in patients with chronic kidney disease (CKD), regardless of the cause of the disease. Increasing evidence from studies based on animal models or human kidney biopsies demonstrates that renal tubular epithelial cells (TECs) induce EMT in response to injuries.[3–10] In addition, transforming growth factor β1 (TGF-β1) has been recognized as the primary factor facilitating the progress of renal fibrosis by eliciting pro-fibrotic effects on target cells and provoking a massive accumulation of the extracellular matrix (ECM).[11] TGF-β1 is a highly potent EMT inducer and has been shown to mediate renal fibrosis by inducing EMT.[12–14]

The *trans*-differentiation of epithelial cells in renal fibrosis does not entirely agree with the features of a complete EMT.[13,15–20] The novel lineage tracing method in a transgenic mouse model indicates that the contribution of TECs to the pool of myofibroblasts is negligible.[12,13,21] Recently, a concept of "partial EMT (pEMT)" (alternatively termed hybrid, intermediate, or incomplete EMT) was proposed to reconcile the role of EMT in kidney fibrosis. The theory of pEMT in kidney fibrosis holds that TECs undergo EMT in response to injuries but fail to acquire complete mesenchymal traits, in which the cells remain attached to the tubular basement membrane.[16–20,22] TECs with pEMT status lose their epithelial identities of apical-basal polarity and intercellular junctions, leading to the disruption of the tubular barrier and dysfunction of solute and solvent transporters,[19] and acquire no potential for migration and regeneration as fibroblasts do.[13,18,19] Moreover, pEMT enables cells to relay pro-fibrotic signals to the interstitium in a paracrine manner.[18,19,23] However, reliable markers of cell pEMT status and the underlying mechanism that redirects pEMT transition in renal fibrosis remain unknown.

During the past decades, a panel of endogenous kidney protective factors possessing antifibrotic capacities, primarily by counteracting the pro-fibrotic effects of TGF-β1, has been identified.[9,24–32] We recently reported a novel TGF-β1 antagonist, JNK-associated leucine zipper protein (JLP, also known as SPAG9),

[1]Department of Nephrology, Renmin Hospital of Wuhan University, Wuhan, China

[2]Department of Nephrology, Minda Hospital, Affiliated with Hubei University for Nationalities, Enshi, China

[3]These authors contributed equally

[4]Lead contact

*Correspondence: rm000301@whu.edu.cn

https://doi.org/10.1016/j.isci.2023.106396

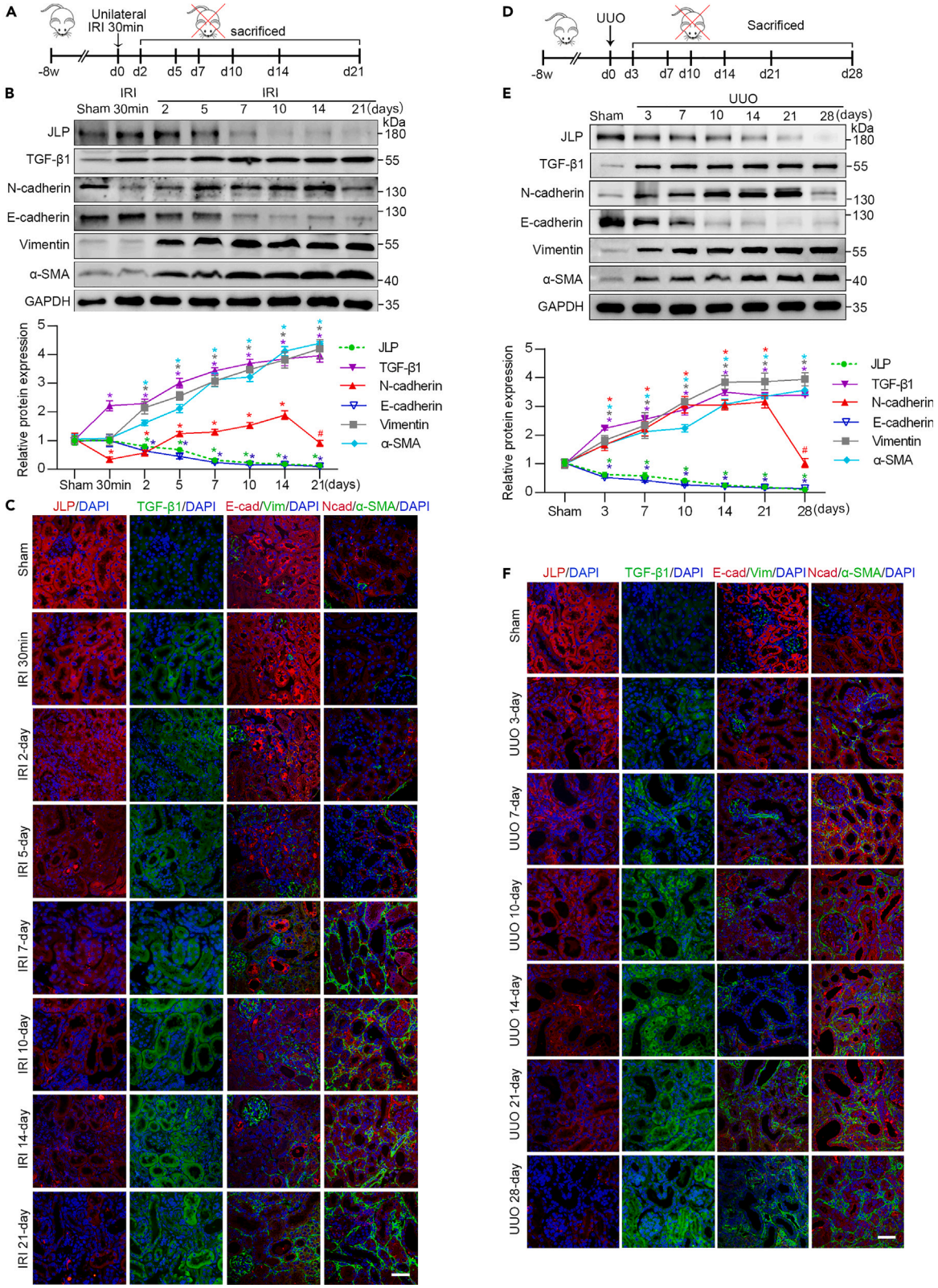
A
Unilateral IRI 30min
sacrificed
-8w
d0 d2 d5 d7 d10 d14 d21
B
IRI
IRI
Sham 30min 2 5 7 10 14 21(days)
kDa
JLP
TGF-β1
N-cadherin
E-cadherin
Vimentin
α-SMA
GAPDH
180
55
130
130
55
40
35
Relative protein expression
JLP
TGF-β1
N-cadherin
E-cadherin
Vimentin
α-SMA
C
JLP/DAPI
TGF-β1/DAPI
E-cad/Vim/DAPI
Ncad/α-SMA/DAPI
Sham
IRI 30min
IRI 2-day
IRI 5-day
IRI 7-day
IRI 10-day
IRI 14-day
IRI 21-day
D
UUO
Sacrificed
-8w
d0 d3 d7 d10 d14 d21 d28
E
UUO
Sham 3 7 10 14 21 28(days)
kDa
JLP
TGF-β1
N-cadherin
E-cadherin
Vimentin
α-SMA
GAPDH
180
55
130
130
55
40
35
Relative protein expression
JLP
TGF-β1
N-cadherin
E-cadherin
Vimentin
α-SMA
F
JLP/DAPI
TGF-β1/DAPI
E-cad/Vim/DAPI
Ncad/α-SMA/DAPI
Sham
UUO 3-day
UUO 7-day
UUO 10-day
UUO 14-day
UUO 21-day
UUO 28-day

Figure 1. Dynamic expression profile of an array of EMT-related molecules in kidney tissues from IRI and UUO mouse models

(A and D) Diagram of the study timeline of the establishment and sacrifice of mouse models for tissue collection.

(B and E) Western blotting of the expression of the indicated proteins in kidney samples harvested at the indicated time point (Left panel) after IRI or UUO induction. The relative abundance of the indicated protein expression was normalized by GAPDH (Right panel). n = 5 mice per group.

(C and F) Representative images (five visual fields for each tissue analyzed) of immunofluorescence staining for the indicated molecules in the kidney samples harvested at the indicated time point after IRI (C) or UUO (F) induction. Scale bars, 50 μm n = 5 mice per group. Quantitative data are expressed as the mean ± S.E.M. two-way ANOVA was applied for two-group comparisons on protein expression in kidney tissues between mice at the indicated timepoint following IRI or UUO induction and mice receiving sham operation. *p< 0.05. EMT, epithelial-mesenchymal transition; IRI, ischemia-reperfusion injury; UOO, unilateral ureteral obstruction; JLP, c-Jun NH2-terminal kinase-associated leucine zipper protein; TGF-β1, transforming growth factor β 1; α-SMA, alpha-smooth muscle actin.

which is predominantly expressed by tubular cells under normal conditions but is substantially downregulated in fibrotic kidney tissues.[32] JLP is a scaffolding protein that regulates mitogen-activated protein kinase signaling pathways belonging to the JIP (JNK interacting protein) family[33] and is a fundamental coordinator of cell vesicle transport.[34–38] The involvement of JLP in multiple cellular processes suggests its critical role in cell fate decisions.[39,40] Ectopic JLP overexpression in various tumors has been reported and is believed to be essential for cell survival, proliferation, migration, and invasion.[41–50] In coordination with TGF-β1, JLP orchestrates EMT that is conducive to tumorigenesis and metastasis.[50–52] We have previously shown that JLP is involved in shaping EMT in TECs and peritoneal mesothelial cells in renal and peritoneal fibrosis, respectively.[32,53] These findings raise the speculation that the dynamic interplay between JLP and TGF-β1 plays a role in the pEMT status of TECs during the progression of kidney fibrosis. In this study, we mapped the temporal expression trajectories of a series of EMT-related molecules in TECs spanning the entire course of renal fibrosis under different genetic backgrounds. We identified N-cadherin as a functional and phenotypic landmark that characterizes the pEMT cell status and proposed the core machinery of JLP-dependent and Foxk1-mediated N-cadherin regulation. Our study demonstrates that N-cadherin downregulation in TECs can be applied to characterize the pEMT state in renal fibrosis.

RESULTS

Temporal trajectory mapping reveals a distinct expression dynamic pattern of N-cadherin in fibrotic kidney tissues

Kidney fibrosis is the chronic pathological destruction of kidney tissues under persistent injury. Although TECs in fibrotic renal tissues are not completely transformed into fibroblasts and are in a state of pEMT that is not conducive to tissue repair, the dynamic change trajectory of the phenotype of TECs in the entire process of renal tissue fibrosis remains unknown. Therefore, we investigated the expression of panel molecules comprising cell phenotypic markers (E-cadherin, N-cadherin, vimentin, and α-smooth muscle actin [α-SMA]) and critical regulators of EMT (TGF-β1 and JLP). Kidney tissues were harvested from mice that underwent renal ischemia-reperfusion injury (IRI) or unilateral ureteral ligation (UUO) and from patients with CKD stages 1,3, or 5 who underwent renal biopsy.

Western blotting showed that 30 min after IRI induction, TGF-β1 expression levels increased sharply. In contrast, N-cadherin expression was downregulated and the expression of other molecules remained unchanged. From 30 min until day 21 after IRI, the expression levels of TGF-β1, vimentin, and α-SMA showed a steady increase whereas those of JLP and E-cadherin showed a stable decrease. The expression of N-cadherin recovered from the short-term decrease at IRI induction, reaching a peak at a high level on the 14th day, and then abruptly plunging to a low level on the 21st day (Figures 1A and 1B). Similar temporal expression trajectories were observed in the unilateral ureteral obstruction (UUO) mouse model, with a steady increase in TGF-β1, vimentin, and α-SMA expression levels, and a stable decrease in JLP and E-cadherin expression levels along with the development of kidney fibrosis. The N-cadherin expression profile showed a surge upon UUO inception, peaking at a high level until the 21st day, and decreasing sharply on the 28th day (Figures 1D and 1E). These dynamic changes in the expression of the indicated molecules in TECs were further confirmed by immunofluorescence (IF) staining in both mouse models (Figures 1C and 1F). As the IRI model adopted in this study included an early phase of acute renal injury and a subsequent phase progressing to chronic kidney fibrosis, the dynamic trajectory of the expression profile 30 min after IRI represents the process of kidney fibrosis (Figures S1A–S1C), which is inconsistent with that in the UUO model.

We further evaluated the expression of these molecules in renal biopsies from patients with CKD stages 1, 3, and 5 using immunohistochemical (IHC) staining (Figure S2A). Semi-quantitative analysis showed a dynamic change trajectory of the indicated molecules, which was inconsistent with the pattern observed in an

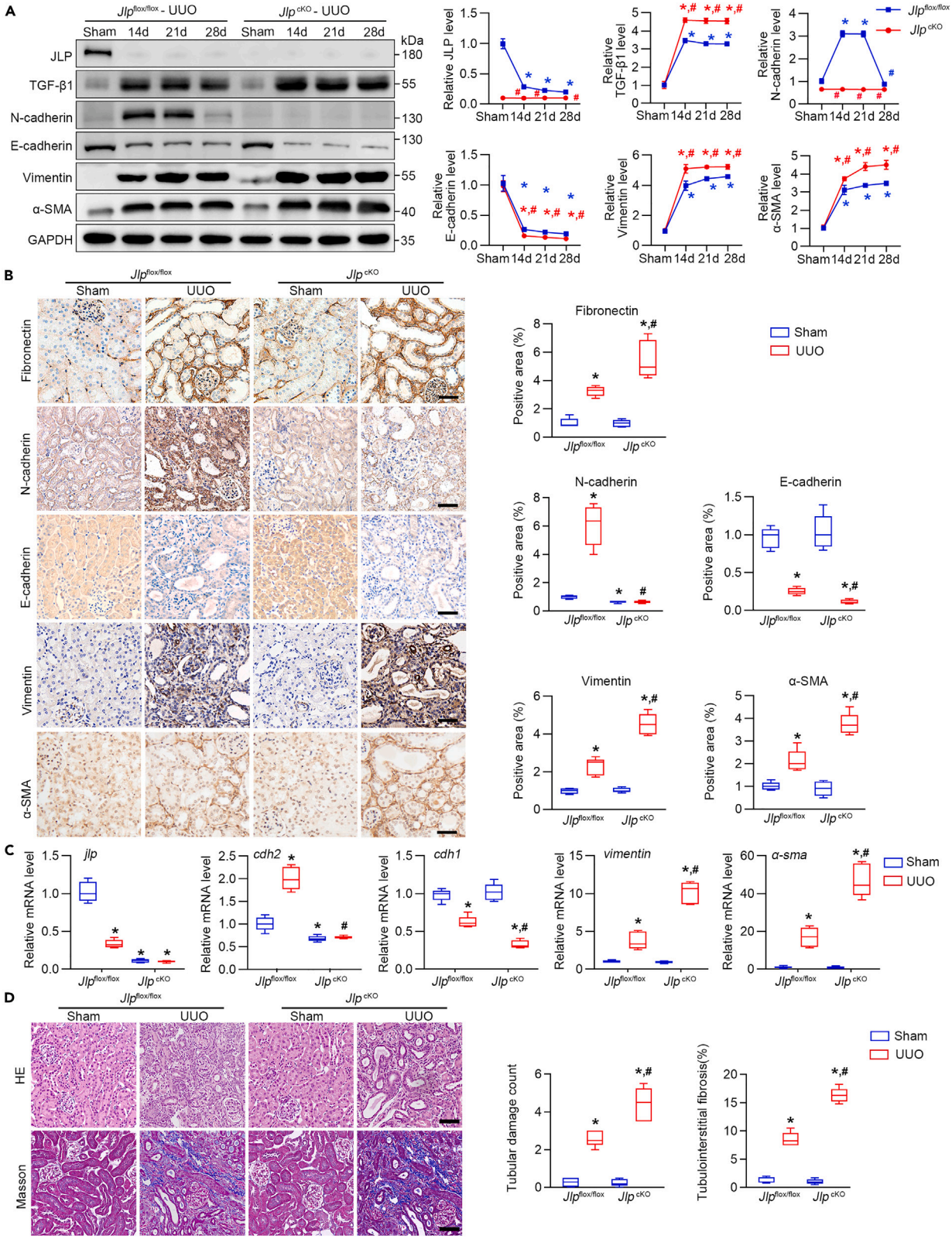
A
Jlp flox/flox - UUO
Jlp cKO - UUO
Sham 14d 21d 28d Sham 14d 21d 28d
kDa
JLP 180
TGF-β1 55
N-cadherin 130
E-cadherin 130
Vimentin 55
α-SMA 40
GAPDH 35
Relative JLP level
Relative TGF-β1 level
Relative N-cadherin level
Relative E-cadherin level
Relative Vimentin level
Relative α-SMA level
Sham 14d 21d 28d
Jlp flox/flox
Jlp cKO
B
Jlp flox/flox
Jlp cKO
Sham UUO Sham UUO
Fibronectin
N-cadherin
E-cadherin
Vimentin
α-SMA
Positive area (%)
Sham
UUO
C
jlp
cdh2
cdh1
vimentin
α-sma
Relative mRNA level
D
HE
Masson
Tubular damage count
Tubulointerstitial fibrosis(%)

Figure 2. JLP deficiency impairs N-cadherin expression and promotes pEMT in tubular cells in UUO-induced renal fibrosis

(A) Western blotting of the dynamic expression of the related molecules in kidney tissues from the UUO mouse model with or without TEC-specific JLP deletion. The relative abundance of the indicated protein expression was normalized by GAPDH (Right panel). n = 5 mice per group.

(B) Representative images (five visual fields for each tissue analyzed) of immunohistochemical staining of the related molecules in kidney tissues from indicated groups and quantification of protein expression. Scale bars, 50 μmn = 5 mice per group.

(C) Quantitative real-time PCR of the Relative JLP mRNA level in kidney tissues from the indicated groups. Data are normalized to GAPDH mRNA level. n = 5 mice per group.

(D) Representative images (five visual fields for each tissue analyzed) of hematoxylin and eosin (HE) and Masson staining of a renal tissue section from indicated groups (left panel) and quantification of the tubular lesion and interstitial fibrosis (right panel). Scale bar, 50 μm. n = 5 per group. Differences in protein or mRNA expression in kidney tissues between different mice models were compared. Quantitative data are expressed as the mean ± S.E.M. *p< 0.05, compared to the sham group; #p< 0.05, compared to $Jlp^{flox/flox}$ mice. pEMT, partial epithelial-mesenchymal transition; JLP, c-Jun NH2-terminal kinase-associated leucine zipper protein; UOO, unilateral ureteral obstruction; TGF-β1, transforming growth factor β 1; α-SMA, alpha-smooth muscle actin.

experimental mouse model (Figure S2B). These results demonstrate that during the progression of renal fibrosis, the dynamic expression trajectory of N-cadherin, which is commonly considered a mesenchymal marker,[54–56] was distinct from that of other markers, displaying a profile of an initial increase followed by a sharp decrease. Therefore, in the late stage of renal fibrosis, N-cadherin is more suitable than other mesenchymal markers to characterize the incomplete phenotypic switch from epithelial to mesenchymal in TECs.

JLP deficiency severely impairs N-cadherin expression in TECs and promotes pEMT in renal fibrosis

Our results indicate that the expression levels of N-cadherin and JLP were downregulated in the late stage of renal fibrosis, which may mark the cell switch to pEMT status corresponding to advanced renal fibrotic lesions. Because JLP functions as an EMT regulator,[32,53] we investigated the relationship between the dynamic changes in JLP and N-cadherin expression levels in kidney fibrosis. We established TEC-specific *Jlp*-knockout mice (Jlp^{cKO}) by crossing transgenic mice with cdh16-Cre mice (Figure S3A) to establish IRI- and UUO-induced renal fibrosis models and investigated the expression of the panel molecules in renal tissue at different time points using western blotting. The results showed that compared to mice expressing JLP normally ($Jlp^{flox/flox}$), Jlp^{cKO} mice undergoing IRI or UUO induction exhibited more robust rising trends of TGF-β1, vimentin, and α-SMA expression levels, whereas N-cadherin remained at a low level during the process, and no early increase was observed (Figures S3B and 2A). Similar results were observed by IHC staining, quantitative polymerase chain reaction (PCR) analysis and IF staining (Figures S3C, S3D, 2B, 2C, and S4). In addition, the renal fibrotic lesion in both mouse models with Jlp^{cKO} was significantly aggravated compared to that in $Jlp^{flox/flox}$ mice (Figures S3E and 2D). These results suggest that in the absence of JLP, TECs lose the ability of inducing N-Cadherin upregulation in response to UUO or IRI challenge, while preserving the potentials of upregulating other mesenchymal markers. Cells under which status distinct to complete EMT transition are closely associated with aggravated renal fibrosis.

We next investigated the regulatory role of JLP in N-cadherin expression and the pEMT state in cultured human renal tubular epithelial cells (HK-2 cells). HK-2 cells with or without JLP knockdown were established by *Jlp*-targeted short hairpin RNA (shRNA) or unrelated control shRNA transfection and were then treated with TGF-β1 or fibroblast growth factor (FGF-2), which are major factors that drive renal fibrosis.[57,58] The dynamic expression profile of the molecules in HK-2 cells treated with TGF-β1 or FGF-2 was analyzed by western blotting (Figures 3A and 3B). We noted a high similarity in the temporal trajectories of molecule cluster expression in cultured HK-2 cells and *in vivo* fibrotic kidney tissues. Briefly, TGF-β1 and FGF-2 induced the upregulation of a panel of mesenchymal markers, including N-cadherin, vimentin, α-SMA, and TGF-β1, in HK-2 cells expressing JLP normally, in contrast to the steady decrease in the expression of E-cadherin and JLP. Notably, N-cadherin expression decreased after 96 h of stimulation, which is distinct from other mesenchymal markers. In addition, *Jlp* shRNA transfection in HK-2 cells severely impaired N-cadherin upregulation in response to TGF-β1 or FGF-2 stimulation whereas the expression of α-SMA was upregulated (Figures 3C–3G). These results from both *in vivo* and *in vitro* studies indicate that TGF-β-induced N-cadherin upregulation in TECs is JLP-dependent, and the loss of JLP in TECs is conducive to the phenotypic transition to pEMT.

Loss of N-cadherin in tubular cells aggravates renal fibrosis

The above results suggest that N-cadherin deficiency following JLP loss in TECs is a hallmark of pEMT in late-stage kidney fibrosis. Therefore, we investigated whether loss of N-cadherin in TECs has considerable pathogenesis. We established tubular-specific conditional *cdh2* knockout mice ($cdh2^{flox/flox}$) by crossing

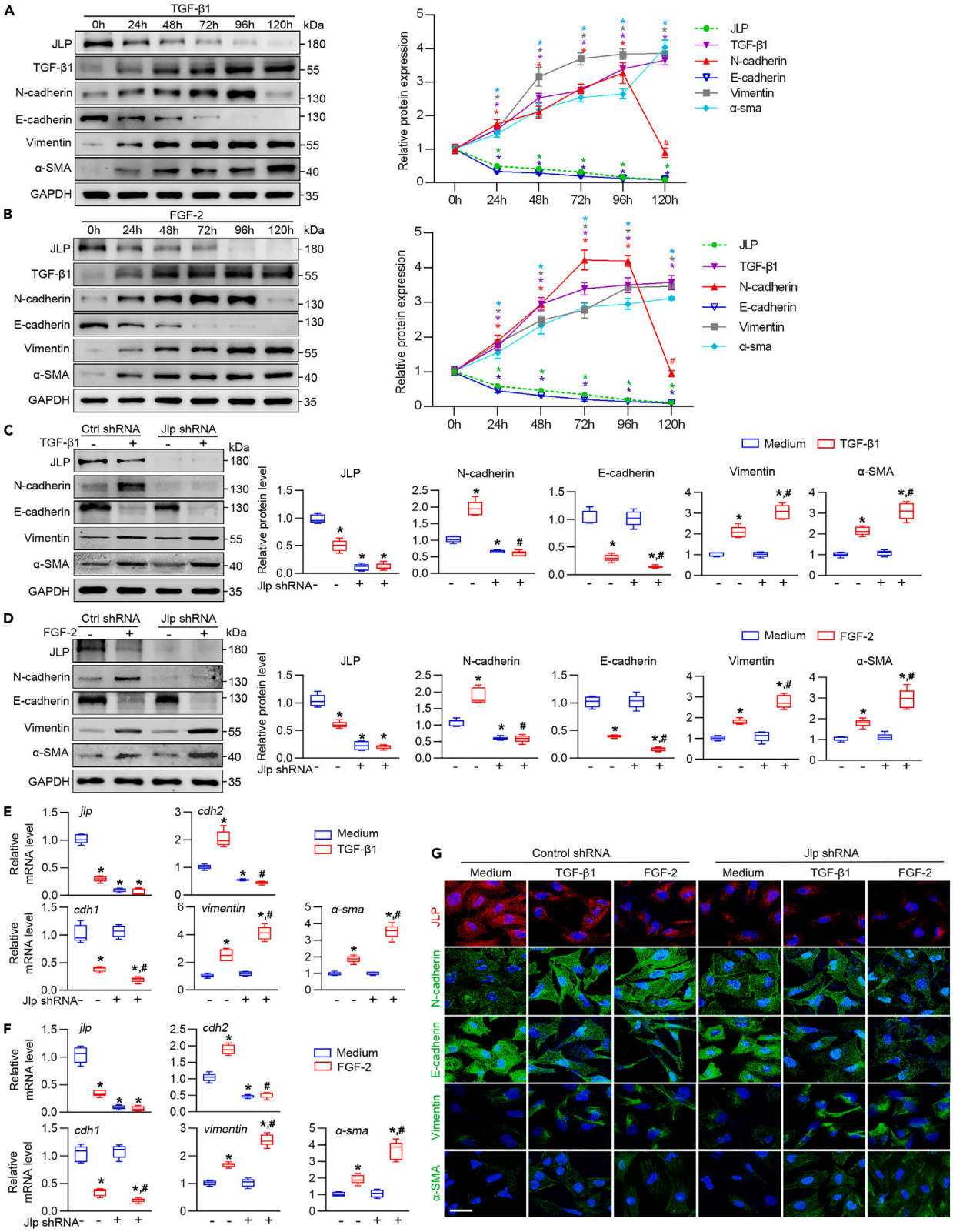
A
TGF-β1
0h 24h 48h 72h 96h 120h kDa
JLP 180
TGF-β1 55
N-cadherin 130
E-cadherin 130
Vimentin 55
α-SMA 40
GAPDH 35
Relative protein expression
JLP
TGF-β1
N-cadherin
E-cadherin
Vimentin
α-sma
B
FGF-2
0h 24h 48h 72h 96h 120h kDa
JLP 180
TGF-β1 55
N-cadherin 130
E-cadherin 130
Vimentin 55
α-SMA 40
GAPDH 35
Relative protein expression
JLP
TGF-β1
N-cadherin
E-cadherin
Vimentin
α-sma
C
Ctrl shRNA
Jlp shRNA
TGF-β1 - + - + kDa
JLP 180
N-cadherin 130
E-cadherin 130
Vimentin 55
α-SMA 40
GAPDH 35
Medium
TGF-β1
JLP
N-cadherin
E-cadherin
Vimentin
α-SMA
Relative protein level
Jlp shRNA - - + +
D
Ctrl shRNA
Jlp shRNA
FGF-2 - + - + kDa
JLP 180
N-cadherin 130
E-cadherin 130
Vimentin 55
α-SMA 40
GAPDH 35
Medium
FGF-2
JLP
N-cadherin
E-cadherin
Vimentin
α-SMA
Relative protein level
Jlp shRNA - - + +
E
jlp
cdh2
cdh1
vimentin
α-sma
Relative mRNA level
Medium
TGF-β1
Jlp shRNA - - + +
F
jlp
cdh2
cdh1
vimentin
α-sma
Relative mRNA level
Medium
FGF-2
Jlp shRNA - - + +
G
Control shRNA
Jlp shRNA
Medium
TGF-β1
FGF-2
Medium
TGF-β1
FGF-2
JLP
N-cadherin
E-cadherin
Vimentin
α-SMA

Figure 3. Dynamic expression profile of an array of EMT-related molecules in HK-2 cells challenged with TGF-β1 or FGF-2

(A–G) HK-2 cells were co-cultured with TGF-β1 or FGF-2 for the indicated time and subjected to western blotting (A and B) to detect the expression of the related proteins (Right panel). The relative abundance of the indicated protein was normalized to GAPDH (Left panel). n = 5 per group. *Jlp* shRNA or control shRNA-transfected HK-2 cells were treated with TGF-β1 or FGF-2 for 48 h and subjected to western blotting (C and D), quantitative real-time PCR (E and F), or immunofluorescent (G) to detect the expression of the related molecules. Representative images (five visual fields for each section analyzed) of immunofluorescence staining (G). Scale bars, 20 μm. n = 5 per group. The relative abundance of the protein or mRNA of the indicated molecules was normalized to GAPDH. n = 5 per group. Differences in protein or mRNA expression in HK-2 cells under the implied conditions were compared. Quantitative data are expressed as the mean ± S.E.M. *p< 0.05, compared to HK-2 cells without TGF-β1 or FGF-2 stimulation; #p< 0.05, compared to HK-2 cells with control shRNA transfection. EMT, epithelial-mesenchymal transition; JLP, c-Jun NH2-terminal kinase-associated leucine zipper protein; UOO, unilateral ureteral obstruction; TGF-β1, transforming growth factor β 1; α-SMA, alpha-smooth muscle actin; FGF-2, fibroblast growth factor 2.

transgenic mice carrying the *cdh2*$^{flox/+}$ with *cdh*16-Cre mice (Figures 4A and 4B), followed by the development of IRI or UUO-induced renal fibrosis mouse models. We observed more severe histological damage in IRI- or UUO-challenged kidneys in *cdh2*^{cKO} mice than in *cdh2*$^{+/+}$ mice, as shown by hematoxylin and eosin (HE) and Masson staining. In addition, the expression of an array of markers of fibrotic lesions, such as fibronectin, collagen-I, vimentin, and α-SMA, which were detected by western blotting in kidney tissues under IRI or UUO challenge, were more increased in *cdh2*^{cKO} mice than in *cdh2*$^{+/+}$ mice (Figures 4C–4F). These histopathological and molecular pathological results suggest that defective expression of N-cadherin in TECs exacerbates the progression of renal fibrosis. These pathological effects of N-cadherin loss were further corroborated in cultured HK-2 cells (Figures S5A and S5B). In *cdh2*-deficient HK-2 cells, which were established by *JLP*-specific shRNA transfection, treatment with TGF-β1 or FGF-2 resulted in increased production of fibronectin, collagen-I, vimentin, and α-SMA compared to control shRNA-transfected HK-2 cells both at the mRNA (Figures S5C and S5D) and protein levels (Figures S5E and S5F). These results indicate that TECs are vulnerable to damaging factors that exert pro-fibrotic effects in the absence of N-cadherin.

Loss of N-cadherin impairs kidney tubular cell survival and growth under pathological conditions

Because loss of N-cadherin in renal tubular cells led to the aggravation of renal fibrosis, we speculated that N-cadherin deficiency might have detrimental effects on TECs in the presence of renal fibrosis. In the kidney tissues of UUO and IRI mouse models with *cdh2*^{cKO}, the number of TECs undergoing apoptosis and G2/M cell-cycle arrest was significantly higher than that in *cdh2*$^{flox/flox}$ mice (Figures S6A and S6B). This phenomenon was also observed in cultured HK-2 cells. TGF-β1 stimulation induced a higher level of apoptosis (Figures 5A and 5B) and G2/M cell-cycle arrest (Figure 5C) in *cdh2*-deficient HK-2 cells compared to control cells. Moreover, the scratch test showed that the migration ability of HK-2 cells was significantly reduced under *cdh2* gene knockdown conditions (Figure 5D). These results demonstrate that in the absence of N-cadherin, TECs are more likely to undergo G2/M cell-cycle arrest during renal fibrosis. Moreover, their cell growth activity and migration ability were significantly reduced, which are key functional features of TECs under the pEMT state in advanced renal fibrosis.[19]

The transcription factor Foxk1 suppresses N-cadherin expression in tubular cells

We investigated the molecular mechanism by which JLP regulates N-cadherin expression. Methylation has been previously reported to be an essential transcriptional regulatory mechanism of N-cadherin.[59] However, our results showed that the methylation state of the N-cadherin promoter in the kidney tissues of the JLP-deficient UUO mouse model was not different from that in the tissues of JLP wild-type mice (Figure 6A). Therefore, because the transcription factor Foxk1 is involved in the regulation of N-cadherin expression,[60,61] we investigated whether JLP affects Foxk1 expression in TECs. We observed that Foxk1 proteins or mRNAs were weakly expressed in kidney tissues of JLP wild-type mice under normal conditions whereas loss of JLP in TECs resulted in the upregulation of Foxk1 at the protein level but not at the mRNA level in kidney tissues (Figures 6B and 6D). Moreover, IRI or UUO challenge led to the accumulation of Foxk1 protein and mRNA levels in kidney tissues of both *Jlp*$^{flox/flox}$ and *Jlp*^{cKO} mice, with *Jlp*^{cKO} mice having higher Foxk1 protein levels but similar mRNA levels compared to *Jlp*$^{flox/flox}$ mice (Figures 6B and 6D).

The effects of JLP and pro-fibrotic factors on Foxk1 expression were further confirmed in cultured HK-2 cells, which were assessed under the indicated conditions (Figures 6C and 6E). Moreover, IF staining showed that TGF-β1 stimulation induced the translocation of Foxk1 from the cytoplasm to the nucleus, which was significantly enhanced after *jlp* knockdown (Figure 6F). The *in vivo* study on the UUO mouse

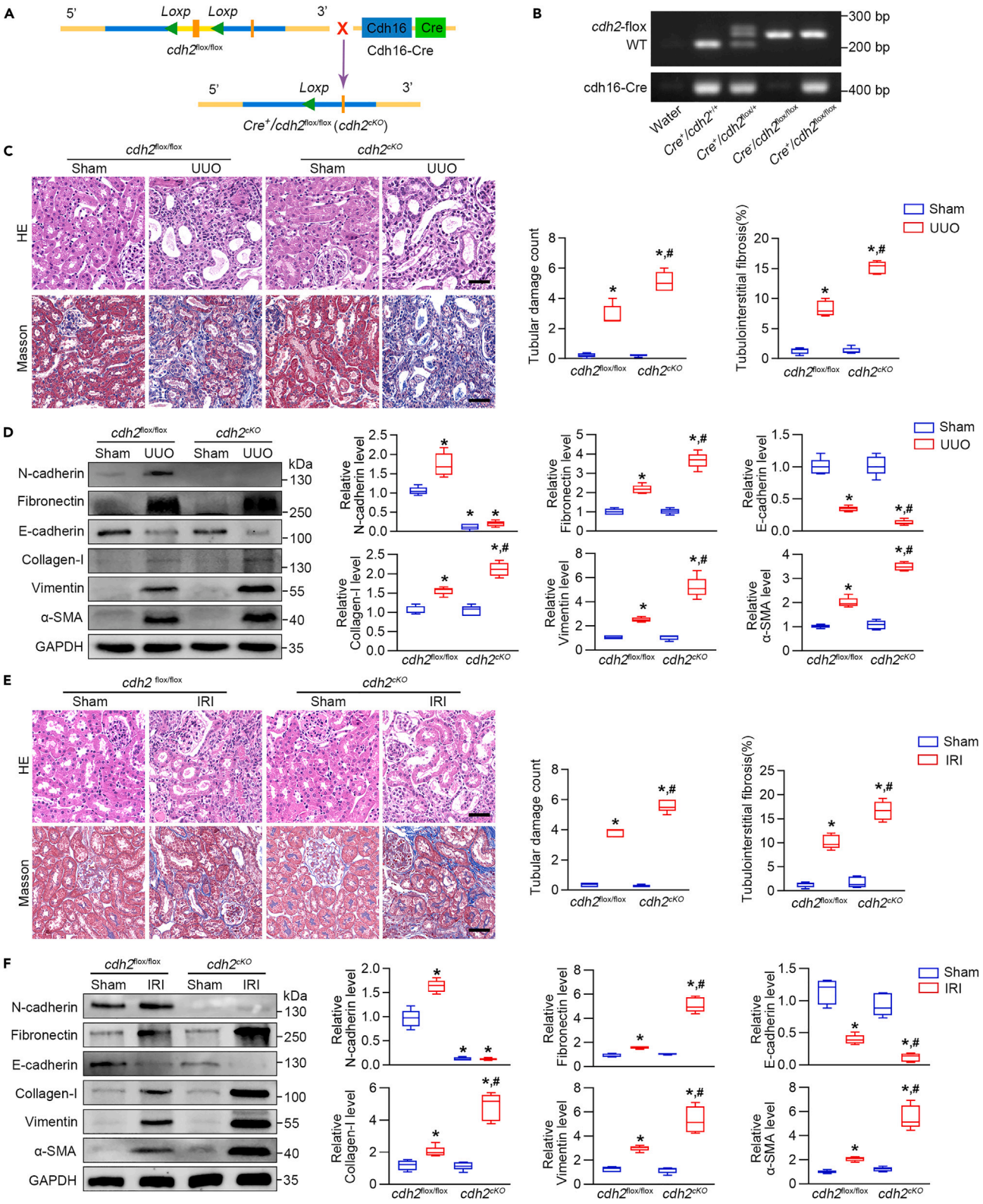

Figure 4. Loss of N-cadherin in tubular cells aggravates renal fibrosis in UUO and IRI mouse models

(A–F) (A and B) Schematic diagram of the generation and identification of TEC-specific N-cadherin knockout mouse ($cdh2^{flox/flox}$) and the control mouse with regular N-cadherin expression ($cdh2^{flox/flox}$). UUO, IRI, or corresponding sham operation was performed on $cdh2^{cKO}$ and $cdh2^{flox/flox}$ mice. Fourteen days

Figure 4. *Continued*

later, the mice were sacrificed for kidney collection. Hematoxylin and eosin (HE) and Masson staining were applied to examine the tubular lesion and interstitial fibrosis in the renal tissue section from the indicated groups (C and E). Scale bar, 50 μm (insets, 10 μm). n = 5 mice per group. Differences in histological changes in kidney tissues between mice under different conditions were compared. Quantitative data are expressed as the mean ± S.E.M. *p< 0.05, compared to the sham group; #p< 0.05, compared with $cdh2^{flox/flox}$ mice. *p< 0.05. Western blotting of the protein expression of the related molecules in kidney tissues from the indicated group (D and F). The relative abundance of the indicated protein expression was normalized to GAPDH. n = 5 mice per group. Differences in protein expression in kidney tissues between mice of different conditions were compared. Quantitative data are expressed as the mean ± S.E.M. *p< 0.05, compared to the sham group; #p< 0.05, compared tp$cdh2^{flox/flox}$ mice. *p< 0.05. pEMT, partial epithelial-mesenchymal transition; JLP, c-Jun NH2-terminal kinase-associated leucine zipper protein; IRI, ischemia-reperfusion injury; UOO, unilateral ureteral obstruction; TEC, tubular epithelial cell; α-SMA, alpha-smooth muscle actin.

model further confirmed the reigning role of JLP on Foxk1 expression and activity (Figure 7E); JLP not only induced Foxk1 expression but also induced its nuclear translocation in TECs, and these effects were significantly more pronounced in Jlp^{cKO} mice.

To investigate whether Foxk1 is involved in the regulation of N-cadherin expression, HK-2 cells with *foxk1* knockdown by *foxk1* shRNA transfection were used to detect N-cadherin expression in response to TGF-β1 or FGF-2 stimulation. Both TGF-β1 and FGF-2 induced N-cadherin protein and mRNA expression in HK-2 cells. These effects were remarkably stronger in *foxk1*-deficient than in cells expressing *foxk1* (Figures 6G–6I), indicating that Foxk1 had a negative regulatory role in N-cadherin expression. These results were also confirmed by a luciferase reporter assay (Figure 6J). Collectively, these results indicate that Foxk1 transcriptionally represses N-cadherin gene expression in tubular cells and that JLP tightly regulates the activities of Foxk1 by downregulating its protein level and delaying its nuclear translocation.

JLP overexpression in tubular cells delays the progression of kidney fibrosis and pEMT transition

The above results demonstrate that the loss of JLP in renal TECs is a critical triggering event in the process of renal fibrosis, which leads to the subsequent activation of Foxk1 signaling and catastrophic loss of N-cadherin. Theoretically, restoring the expression of JLP in TECs would mitigate these adverse effects. To investigate this theory, we constructed a transgenic mouse (Jlp^{TG} mouse) with TEC-specific JLP overexpression (Figure 7A) and established a UUO mouse model using Jlp^{TG} and Jlp^{WT} mice. The degree of renal fibrosis damage in Jlp^{TG} mice was significantly alleviated compared to that in Jlp^{WT} mice (Figure 7B). IF and western blot analyses showed that α-SMA and vimentin expression levels were considerably decreased. In contrast, the expression of N-cadherin was significantly upregulated in the tubular cells of Jlp^{TG} mice compared to that in the cells of Jlp^{WT} mice, suggesting that JLP expression in renal TECs was effective in mitigating the pEMT status in the experimental kidney fibrosis model (Figures 7C and 7E). Furthermore, the protective role of JLP overexpression on TGF-β1-induced pro-fibrotic effects was verified in cultured HK-2 cells, which was manifested by changes in the expression of a panel of the related molecules (Figure 7D). In addition, the beneficial effects of JLP overexpression on mitigating Foxk1 expression and nuclear translocation were also observed in cultured HK-2 cells and the UUO mouse model (Figures 7C–7E).

DISCUSSION

Renal fibrosis, a destructive pathologic lesion caused by relentless injury, is characterized by interstitial inflammation, myofibroblasts proliferation, ECM accumulatio, and loss of interstitial capillary integrity. Many cell types and molecules have been found involved in the process of renal fibrosis, and they form a very complex interaction network. ECM components are mainly produced by myofibroblasts,[11] the origin of which are residential fibroblasts, fibrocytes, pericytes, endothelial cells, and etc. Although only very few TECs undergo complete EMT and become Myofibroblast, the abnormalities in phenotype and functions of TECs play a key role in promoting the progress of renal fibrosis.[13] EMT is triggered in TECs in a context-dependent manner as a response to injury, resulting in either physiological tissue repair or kidney fibrosis. TGF-β1 is a potent inducer of EMT and the primary driver of kidney fibrosis. Intriguingly, TECs undergo EMT during renal fibrosis progression but fail to acquire total mesenchymal traits. JLP is a newly identified antifibrotic molecule that counteracts the pro-fibrotic effects of TGF-β1. The present study aimed to determine the temporal trajectory of the EMT phenotypic evolution of tubular cells during renal fibrosis progression and to identify the markers characterizing the transition to the pEMT state. Dynamic profiling of the expression of relevant molecules in kidney tissues from patients with CKD1-5 stage or mouse models revealed a decreasing trend of JLP expression and a stable increasing trend of TGF-β1, α-SMA, and vimentin

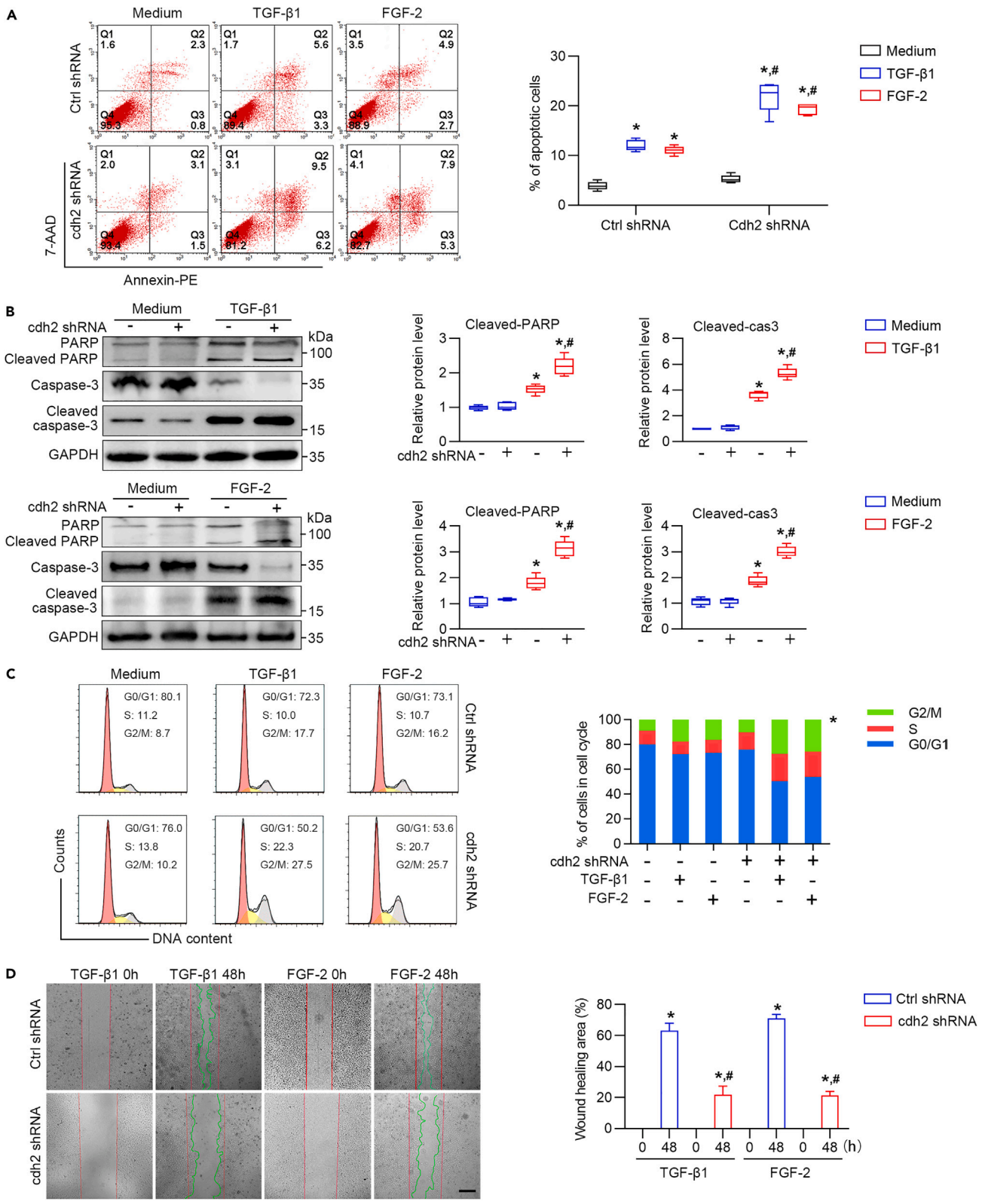
A
Medium
TGF-β1
FGF-2
Ctrl shRNA
cdh2 shRNA
7-AAD
Annexin-PE
Q1 1.6
Q2 2.3
Q4 95.3
Q3 0.8
Q1 1.7
Q2 5.6
Q4 89.4
Q3 3.3
Q1 3.5
Q2 4.9
Q4 88.9
Q3 2.7
Q1 2.0
Q2 3.1
Q4 93.4
Q3 1.5
Q1 3.1
Q2 9.5
Q4 81.2
Q3 6.2
Q1 4.1
Q2 7.9
Q4 82.7
Q3 5.3
% of apoptotic cells
Ctrl shRNA
Cdh2 shRNA
Medium
TGF-β1
FGF-2
B
cdh2 shRNA
PARP
Cleaved PARP
Caspase-3
Cleaved caspase-3
GAPDH
kDa
100
35
15
35
Medium
TGF-β1
FGF-2
Relative protein level
Cleaved-PARP
Cleaved-cas3
C
G0/G1: 80.1
S: 11.2
G2/M: 8.7
G0/G1: 72.3
S: 10.0
G2/M: 17.7
G0/G1: 73.1
S: 10.7
G2/M: 16.2
G0/G1: 76.0
S: 13.8
G2/M: 10.2
G0/G1: 50.2
S: 22.3
G2/M: 27.5
G0/G1: 53.6
S: 20.7
G2/M: 25.7
Counts
DNA content
% of cells in cell cycle
G2/M
S
G0/G1
D
TGF-β1 0h
TGF-β1 48h
FGF-2 0h
FGF-2 48h
Wound healing area (%)
Ctrl shRNA
cdh2 shRNA
0 48 0 48 0 48 0 48 (h)
TGF-β1
FGF-2

Figure 5. Effect of N-cadherin deficiency on apoptosis, cell cycle, and migratory abilities in response to TGF-β1 or FGF-2 stimulation in HK-2 cells

(A) HK-2 cells with *cdh2* short hairpin (sh) RNA or controlled shRNA transfection were treated with TGF-β1 or FGF-2 and then subjected to flow cytometry to evaluate apoptosis using 7-AAD/Annexin-PE staining (left panel). The proportion of apoptotic cells in different groups was counted and compared. n = 5 per group. (B) Western blotting of apoptotic proteins in the above-described HK-2 cells. The relative abundance of the protein was normalized to GAPDH. n = 5 per group.

(C) The cell cycle was analyzed on the above-described HK-2 cells. The percentage of cells at the indicated cell cycle stage was counted and compared. n = 5 per group.

(D) To evaluate cell motility, a scratch test was performed on the above-described HK-2 cells. The gaps in wound healing were measured and compared. Scale bar, 50 μm. n = 3 per group. Quantitative data are expressed as the mean ± S.E.M. *p < 0.05, compared to HK-2 cells without TGF-β1 or FGF-2 stimulation; #p< 0.05, compared with HK-2 cells with mock shRNA transfection. TGF-β1, transforming growth factor β 1; FGF-2, fibroblast growth factor 2.

expression, whereas N-cadherin exhibited distinct expression trajectory of an initial increase and a final decrease. Moreover, loss of JLP in TECs severely impaired N-cadherin induction in response to injuries but enhanced the expression of other mesenchymal markers, such as α-SMA and vimentin. TEC-specific N-cadherin knockout aggravated fibrotic kidney lesions, indicating the pathological significance of N-cadherin downregulation mediated by Foxk1 via a negative transcriptional mechanism. JLP shores up the increase in N-cadherin in TECs as a repair response to injuries during the early phase of renal fibrosis by suppressing Foxk1 protein expression and its nuclear translocation. This study suggests that Foxk1 up-regulation and N-cadherin downregulation in advanced fibrotic kidneys can be effectively reversed by TEC-specific JLP overexpression, providing novel strategies for preventing renal fibrosis.

Description of the phenotypic alteration of TECs during the progression of kidney fibrosis is crucial to avoid static interpretation of cell fate differentiation. In the present study, by detecting the expression levels of JLP and other related molecules in the kidney tissues of a mouse model and patients with CKD at different stages of kidney fibrosis, we drew temporal trajectories reflecting the dynamic trends of the relevant factors and noted a distinct alteration pattern of increasing and decreasing N-cadherin levels. Because N-cadherin is critical for the survival of TECs under fibrotic lesions, it is reasonable to highlight the turning point of N-cadherin expression from an upregulated to a downregulated state in the later stages of renal fibrosis, which may signal the formation of pEMT states in TECs. We propose that pEMT homeostasis of TECs can be characterized by composite indicators of N-cadherin combined with E-cadherin, α-SMA, or vimentin expression levels. For example, the double low expression of N-cadherin and E-cadherin (N-cadherin^{low}/E-cadherin^{low}), low expression of N-cadherin and high expression of α-SMA (N-cadherin^{low}/α-SMA^{high}), or low expression of N-cadherin and increased expression of vimentin (N-cadherin^{low}/Vimentin^{high}) in TECs can all be used as hallmarks of pEMT states. However, because α-SMA and vimentin are also expressed in other cell types, such as fibroblasts or smooth muscle cells, we recommend N-cadherin^{low}/E-cadherin^{low} as the preferred indicator. However, this indicator does not necessarily apply to characterize other fibrotic diseases because fundamental knowledge of the respective conditions is still lacking.

In the present study, we found that JLP downregulation in TECs occurred earlier than that of N-cadherin in the process of renal fibrosis. Knockdown of the *JLP* gene in renal TECs *in vivo* or *in vitro* caused the cells to lose the ability to induce N-cadherin expression but upregulated the expression of α-SMA and vimentin, indicating that N-cadherin upregulation is JLP-dependent. JLP does not directly facilitate the expression of N-cadherin but tightly controls the activity of the transcription factor Foxk1. When JLP is lost, Foxk1 is upregulated to repress N-cadherin transcription. Therefore, there exists a JLP-Foxk1-N-cadherin signaling axis in renal TECs, which, together with TGF-β1, forms a network motif to regulate N-cadherin expression (Figure 8). In this study, the expression of α-SMA and vimentin in TECs was stably upregulated under the action of pro-fibrotic factors after JLP downregulation, suggesting that JLP inhibits the TGF-β1-induced expression of α-SMA and vimentin. However, further studies are needed to determine whether Foxk1 is involved in this regulation. In addition, the mechanism of JLP blocking Foxk1 protein expression and nuclear translocation is a concerning issue that needs to be investigated.

High levels of ectopic JLP expression have been reported in various tumor cells. JLP plays a pivotal role in tumor cell survival, proliferation, and metastasis, and has been recognized as a reliable prognostic biomarker and potential therapeutic target for patients with cancer. Moreover, JLP plays a crucial role in shaping the EMT phenotype of tumor cells by promoting the expression of a panel of proteins, including Snail1, Twist, vimentin, and N-cadherin.[50–52] N-cadherin expression in tumor cells plays a major role in metastasis.[62] Therefore, the findings that abundant JLP exists in tumor tissues and the contrasting JLP deficiency in fibrotic tissues may explain the fundamental difference in cell fate decisions between tumors and

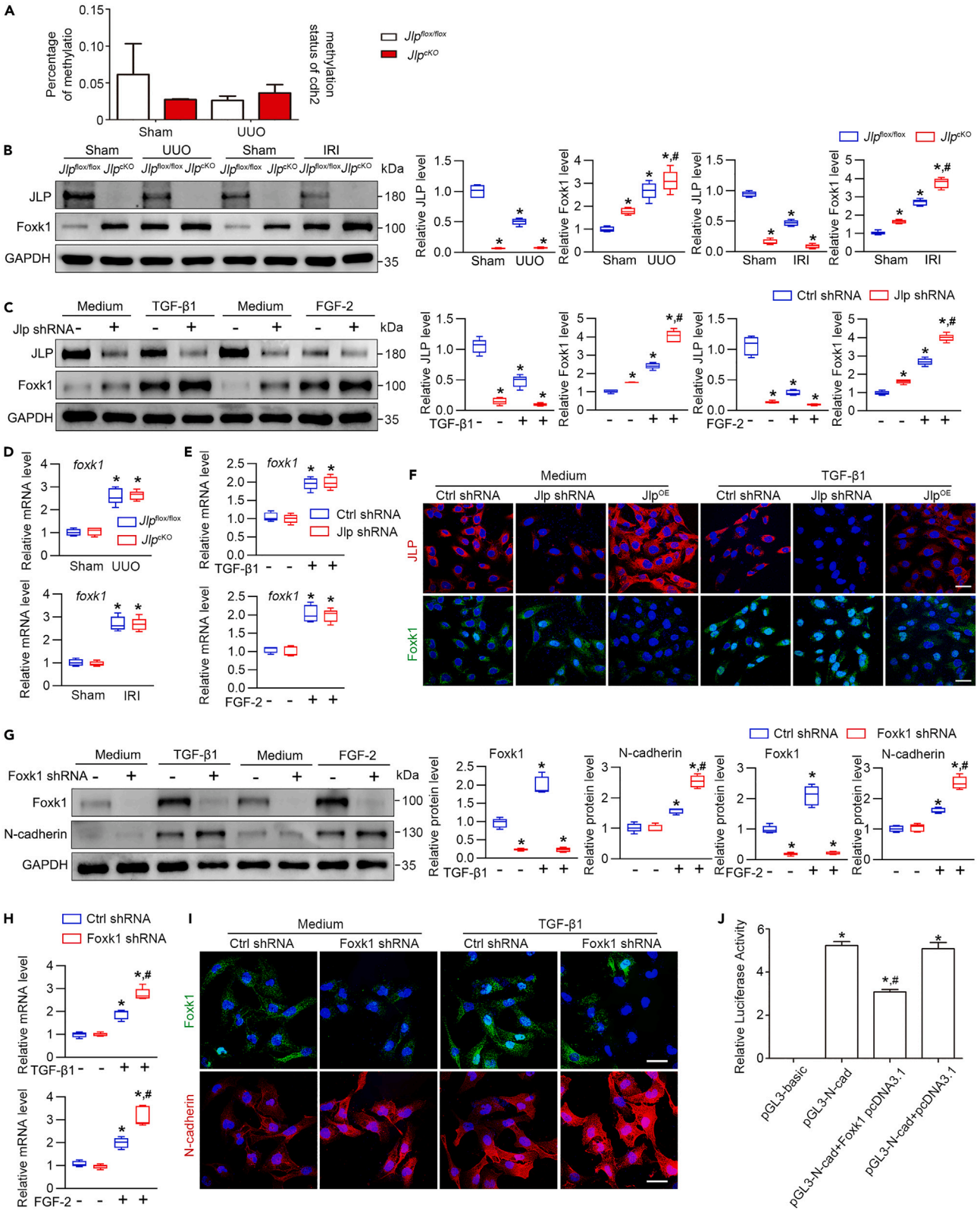
A
Percentage of methylatio
methylation status of cdh2
Sham
UUO
B
Sham
UUO
Sham
IRI
JLP
Foxk1
GAPDH
kDa
180
100
35
Relative JLP level
Relative Foxk1 level
C
Medium
TGF-β1
Medium
FGF-2
Jlp shRNA
Ctrl shRNA
Jlp shRNA
TGF-β1
FGF-2
D
foxk1
Relative mRNA level
Sham
UUO
IRI
E
F
Medium
TGF-β1
Ctrl shRNA
Jlp shRNA
JlpOE
JLP
Foxk1
G
Foxk1 shRNA
N-cadherin
Relative protein level
H
I
J
Relative Luciferase Activity
pGL3-basic
pGL3-N-cad
pGL3-N-cad+Foxk1 pcDNA3.1
pGL3-N-cad+pcDNA3.1

Figure 6. The role of the transcription factor Foxk1 in JLP-dependent N-cadherin expression in tubular cells

(A) The methylation status of the *cdh2* gene was evaluated in kidney tissues from the UUO mice model with $Jlp^{flox/flox}$ or Jlp^{cKO}.

(B and D) Western blot and quantitative real-time PCR analyses of the protein or mRNA expression levels of N-cadherin and Foxk1, respectively, in kidney tissues from UUO mice with $Jlp^{flox/flox}$ or Jlp^{cKO}. The relative abundance of the proteins or mRNAs was normalized to GAPDH. n = 5 mice per group.

(C and E) Western blot and quantitative real-time PCR analyses of the protein or mRNA expression levels of N-cadherin and Foxk1, respectively, in TGF-β1 or FGF-2-stimulated HK-2 cells with *Jlp* shRNA or mock shRNA transfection.

(F) shRNA sequence targeting the *foxk1* gene with high silencing effects was screened.

(G–I) Western blot and quantitative real-time PCR analyses of the protein or mRNA expression levels of N-cadherin, respectively, in TGF-β1- or FGF-2-stimulated HK-2 cells with *foxk1* shRNA or mock shRNA transfection. The relative abundance of the protein or mRNA was normalized to GAPDH. Scale bar, 20 μmn = 5 per group. The difference in protein or mRNA expression in HK-2 cells under the indicated conditions was compared. Quantitative data are expressed as the mean ± S.E.M. *p< 0.05, compared to HK-2 cells without TGF-β1 or FGF-2 stimulation; #p< 0.05, compared to HK-2 cells with mock shRNA transfection.

(J) Luciferase reporter assay was used to analyze the transcriptional role of foxk1 on *cdh2* gene expression. The relative luciferase activity is expressed as the mean ± S.E.M. *p< 0.05, compared with the pGL3-basic group; #p< 0.05, compared with the pGL3-N-cad or pGL3-N-cad + pcDNA3.1 groups. TGF-β1, transforming growth factor β 1; FGF-2, fibroblast growth factor 2; IRI, ischemia-reperfusion injury; UOO, unilateral ureteral obstruction; JLP, c-Jun NH2-terminal kinase-associated leucine zipper protein.

degenerative diseases. In addition, tumor cells in the pEMT state exhibiting highly invasive and highly metastatic potential have also been reported.[63–66] Unlike TECs in renal fibrosis, these tumor cells undergoing pEMT expressed both epithelial phenotypic markers, such as E-cadherin, and mesenchymal markers, such as vimentin and N-cadherin. Retaining E-cadherin expression in tumor cells enables cell survival and collective cell invasion instead of individual cell migration.[67] Therefore, we speculate that the pEMT state of tumor cells is starkly different from that of epithelial cells in tissue fibrosis; the former shows a double high expression level of epithelial (E-cadherin) and mesenchymal markers (N-cadherin) whereas the latter exhibits a double dim expression of E-cadherin and N-cadherin.

EMT has been traditionally considered a binary switch. However, co-expression of epithelial and mesenchymal markers within the same tumor cells has been reported.[68–72] Our findings of weak to no expression of the epithelial marker E-cadherin and mesenchymal marker N-cadherin TECs support that EMT may proceed in a diverse manner depending on the pathological conditions. During the entire course of renal fibrosis, TECs undergo a phenotypic transition from the epithelial cell type (E-cadherin^{high}/N-cadherin^{low}) to the mesenchymal-like cell type (E-cadherin^{low}/N-cadherin^{high}) in the early stage and ultimately switch to the pEMT state (E-cadherin^{low}/N-cadherin^{low}) in the late stage. This dynamic course strongly suggests that the pEMT state in renal fibrosis is formed after the full EMT transition and is not the intermediate state between epithelial and mesenchymal cells as in tumor cells. The short period of tubular cells attaining full mesenchymal attributes allows rare cells to successfully transform into migratory fibroblasts.[12,13,21] In our study, the time-course trajectory analysis showed that EMT proceeds with a shift in the balance between TGF-β1 and JLP. These findings suggest that JLP, as a renal endogenous antifibrotic factor and TGF-β1 antagonist, acts as a checkpoint of the EMT continuum in TECs during renal fibrosis progression.

Limitations of the study

This study found that JLP regulates Foxk1 protein level and transcriptional activity, but the underlying mechanisms have not been adequately elucidated.

STAR★METHODS

Detailed methods are provided in the online version of this paper and include the following:

- KEY RESOURCES TABLE
- RESOURCE AVAILABILITY
  - Lead contact
  - Materials availability
  - Data and code availability
- EXPERIMENTAL MODEL AND SUBJECT DETAILS
  - Mice models
  - Human biopsy specimens
  - Cell culture and treatment
- METHOD DETAILS
  - Histopathology and immunohistochemistry

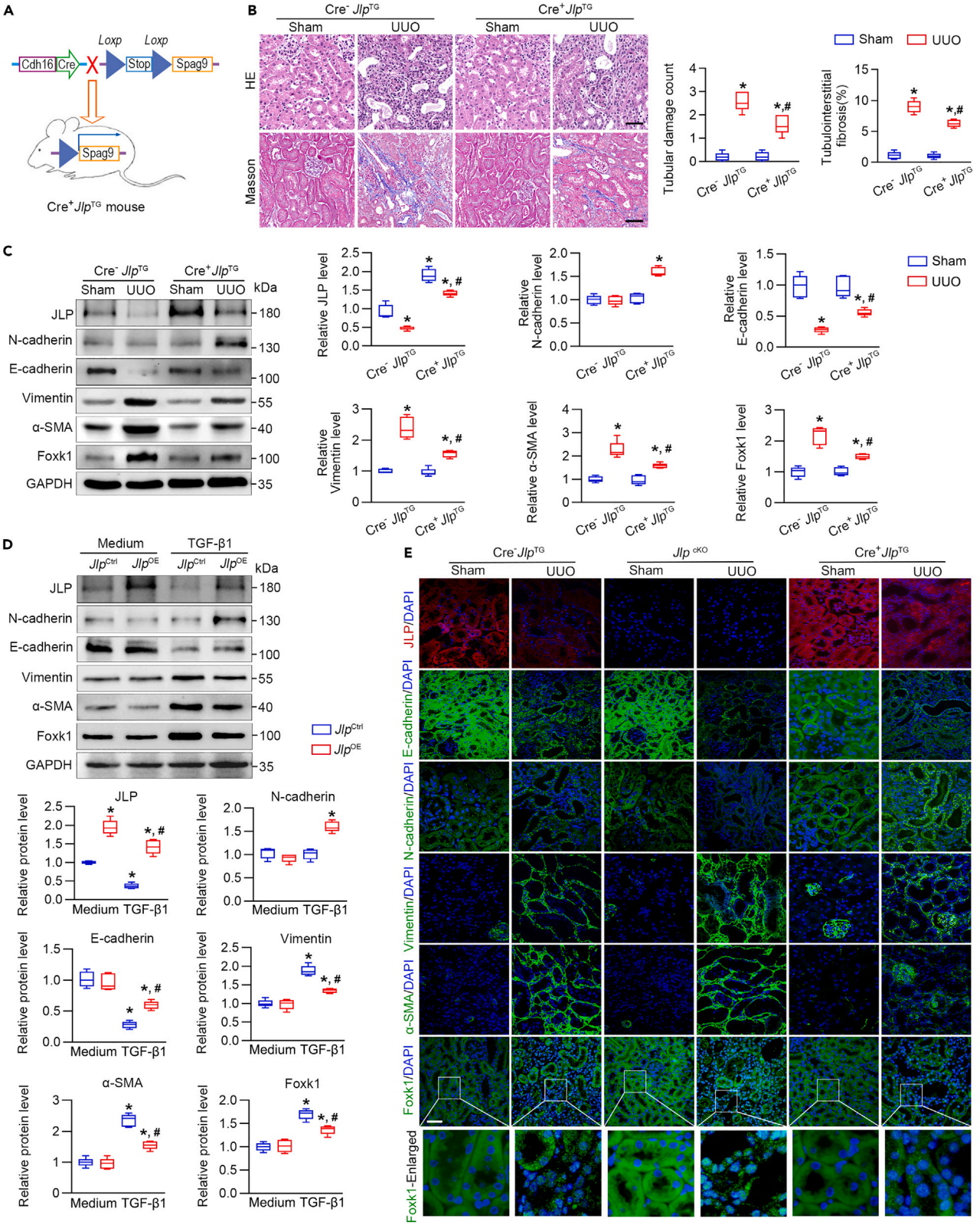
A
Loxp
Loxp
Cdh16 Cre
Stop
Spag9
Spag9
Cre+ Jlp TG mouse
B
Cre- Jlp TG
Cre+ Jlp TG
Sham
UUO
HE
Masson
Tubular damage count
Tubulointerstitial fibrosis(%)
C
JLP
N-cadherin
E-cadherin
Vimentin
α-SMA
Foxk1
GAPDH
kDa
Relative JLP level
Relative N-cadherin level
Relative E-cadherin level
Relative Vimentin level
Relative α-SMA level
Relative Foxk1 level
D
Medium
TGF-β1
Jlp Ctrl
Jlp OE
Relative protein level
E
Jlp cKO
JLP/DAPI
E-cadherin/DAPI
N-cadherin/DAPI
Vimentin/DAPI
α-SMA/DAPI
Foxk1/DAPI
Foxk1-Enlarged

Figure 7. JLP overexpression of in tubular cells ameliorates lesions of renal fibrosis and delays pEMT

(A) Diagram the generated TEC-specific *Jlp* knock-in mouse ($Cre^{+}Jlp^{TG}$) and the control mouse with normal JLP expression ($Cre^{-}Jlp^{TG}$).

(B) Hemotoxylin and eosin and Masson staining of the tubular lesion and interstitial fibrosis in the renal tissue section from UUO mice with $Cre^{+}Jlp^{TG}$ or $Cre^{-}Jlp^{TG}$. Scale bar, 50 μm. n = 5 mice per group.

(C) Western blotting of the expression of the related proteins in kidney tissues from UUO mice with $Cre^{+}Jlp^{TG}$ or $Cre^{-}Jlp^{TG}$. The relative abundance of the indicated protein was normalized to GAPDH. Scale bar, 50 μm. n = 5 mice per group.

(D) Western blotting of the expression of the related proteins in Jlp^{OE}- or Jlp^{Ctrl}-transfected HK-2 cells with or without TGF-β1 stimulation. The relative abundance of the indicated protein was normalized toGAPDH. n = 5 per group.

(E) Representative images of immunofluorescence staining the related molecules in renal tissue sections from the indicated mice. Scale bar, 50 μm. Differences in protein expression in kidney tissues between mice were compared. Quantitative data are expressed as the mean ± S.E.M. *p< 0.05, compared to the sham group; #p< 0.05, compared to $Cre^{-}Jlp^{TG}$ mice. *p< 0.05. pEMT, partial epithelial-mesenchymal transition; TEC, tubular epithelial cell; JLP, c-Jun NH2-terminal kinase-associated leucine zipper protein; α-SMA, alpha-smooth muscle actin.

- Immunofluorescence staining
- Western blotting
- Quantitative real-time PCR (qRT-PCR)
- Cell migration assay
- Methylated DNA immunoprecipitation (MeDIP) assay

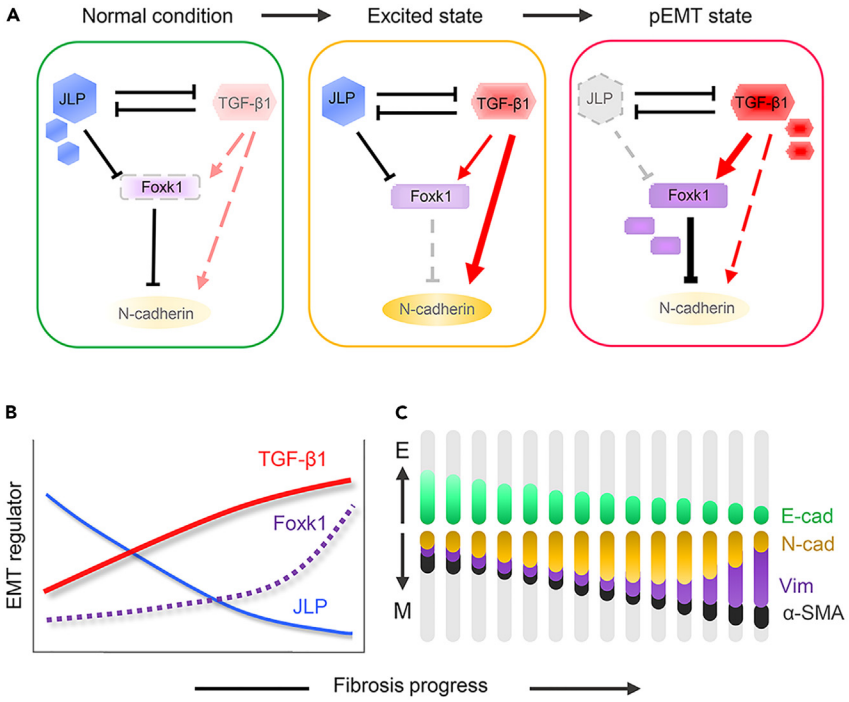

Figure 8. Schematic diagram of the JLP/Foxk1/N-cadherin axis in fostering tubular cell pEMT status

(A) The core machinery that regulates N-cadherin expression involves the interplay between TGF-β1, JLP, and Foxk1 in TECs. JLP reciprocally counteracts TGF-β1, which can induce N-cadherin and Foxk1 expression. The transcription factor Foxk1 acts as a repressor of N-cadherin but is tightly regulated by JLP. Under normal conditions, JLP is expressed by renal TECs, whereas TGF-β1, Foxk1, and N-cadherin are weakly expressed. Under pathological conditions caused by various injuries, the activation of the TGF-β1 signaling pathway promotes N-cadherin and Foxk1 expression. In the presence of JLP, Foxk1 is blocked from suppressing N-cadherin expression, allowing the upregulation of N-cadherin in TECs as an adaptive response to damage. The persistent injuries result in the loss of JLP in TECs, thereby leading to the unleashing of Foxk1. Foxk1 overactivation substantially represses the N-cadherin expression, a sign marking the pEMT state.

(B) Dynamic alteration of core EMT regulators, JLP, TGF-β1, and Foxk1, in TECs during the progress of renal fibrosis.

(C) Dynamic alteration of relevant phenotypic markers of EMT state in TECs during the progress of renal fibrosis. The decrease in N-cadherin is a landmark featuring the pEMT condition of tubular cells in the progression of renal fibrosis.

pEMT, partial epithelial-mesenchymal transition; IRI, ischemia-reperfusion injury; UOO, unilateral ureteral obstruction; JLP, c-Jun NH2-terminal kinase-associated leucine zipper protein; TGF-β1, transforming growth factor β 1; α-SMA, alpha-smooth muscle actin; TEC, tubular epithelial cell.

- Luciferase reporter assay
- Flow cytometric analysis

- QUANTIFICATION AND STATISTICAL ANALYSIS

SUPPLEMENTAL INFORMATION

Supplemental information can be found online at https://doi.org/10.1016/j.isci.2023.106396.

ACKNOWLEDGMENTS

This work was supported by grants from the National Natural Science Foundation of China (NSFC) to Dr. Huiming Wang (No. 82270711), Dr. Lu Zhang (No. 81800614), Hubei Province Major Scientific and Technological Special Project to Dr. Huiming Wang (No. 2019ACA137), and the China Population Welfare Foundation to Dr. Huiming Wang (No. SLB-6-20210323-99). Statement of ethics: All protocols were approved by the Animal Ethics Review Board of Wuhan University (Approval No. WDRM-20211102) and the Ethics Committee of the Renmin Hospital of Wuhan University for Clinical Research (Approval No. WDRY2021-KS045). All protocols were performed in accordance with the guidelines of the National Health and Medical Research Council of China.

AUTHOR CONTRIBUTIONS

L.Z. and H.W. conceived and designed the study. M.T., L.Z., and S.L. performed the experiments. M.Z., B.X., C.L., Y.S., and L.Z. collected the clinical files. M.T., S.L., and L.Q. analyzed and organized the data. H.W. wrote the paper.

DECLARATION OF INTERESTS

The authors declare no competing interests.

INCLUSION AND DIVERSITY

We support inclusive, diverse, and equitable conduct of research.

Received: December 19, 2022
Revised: February 16, 2023
Accepted: March 9, 2023
Published: March 14, 2023

REFERENCES

1. Nieto, M.A., Huang, R.Y.J., Jackson, R.A., and Thiery, J.P. (2016). Emt: 2016. Cell *166*, 21–45. https://doi.org/10.1016/j.cell.2016.06.028.

2. Skrypek, N., Goossens, S., De Smedt, E., Vandamme, N., and Berx, G. (2017). Epithelial-to-mesenchymal transition: epigenetic reprogramming driving cellular plasticity. Trends Genet. *33*, 943–959. https://doi.org/10.1016/j.tig.2017.08.004.

3. Higgins, D.F., Kimura, K., Bernhardt, W.M., Shrimanker, N., Akai, Y., Hohenstein, B., Saito, Y., Johnson, R.S., Kretzler, M., Cohen, C.D., et al. (2007). Hypoxia promotes fibrogenesis in vivo via HIF-1 stimulation of epithelial-to-mesenchymal transition. J. Clin. Invest. *117*, 3810–3820. https://doi.org/10.1172/JCI30487.

4. Inoue, T., Okada, H., Takenaka, T., Watanabe, Y., and Suzuki, H. (2009). A case report suggesting the occurrence of epithelial-mesenchymal transition in obstructive nephropathy. Clin. Exp. Nephrol. *13*, 385–388. https://doi.org/10.1007/s10157-009-0168-4.

5. Iwano, M., Plieth, D., Danoff, T.M., Xue, C., Okada, H., and Neilson, E.G. (2002). Evidence that fibroblasts derive from epithelium during tissue fibrosis. J. Clin. Invest. *110*, 341–350. https://doi.org/10.1172/JCI15518.

6. Nishitani, Y., Iwano, M., Yamaguchi, Y., Harada, K., Nakatani, K., Akai, Y., Nishino, T., Shiiki, H., Kanauchi, M., Saito, Y., and Neilson, E.G. (2005). Fibroblast-specific protein 1 is a specific prognostic marker for renal survival in patients with IgAN. Kidney Int. *68*, 1078–1085. https://doi.org/10.1111/j.1523-1755.2005.00500.x.

7. Rastaldi, M.P., Ferrario, F., Giardino, L., Dell'Antonio, G., Grillo, C., Grillo, P., Strutz, F., Müller, G.A., Colasanti, G., and D'Amico, G. (2002). Epithelial-mesenchymal transition of tubular epithelial cells in human renal biopsies. Kidney Int. *62*, 137–146. https://doi.org/10.1046/j.1523-1755.2002.00430.x.

8. Strutz, F., Zeisberg, M., Ziyadeh, F.N., Yang, C.Q., Kalluri, R., Müller, G.A., and Neilson, E.G. (2002). Role of basic fibroblast growth factor-2 in epithelial-mesenchymal transformation. Kidney Int. *61*, 1714–1728. https://doi.org/10.1046/j.1523-1755.2002.00333.x.

9. Zeisberg, M., Hanai, J.i., Sugimoto, H., Mammoto, T., Charytan, D., Strutz, F., and Kalluri, R. (2003). BMP-7 counteracts TGF-beta1-induced epithelial-to-mesenchymal transition and reverses chronic renal injury. Nat. Med. *9*, 964–968. https://doi.org/10.1038/nm888.

10. Nadasdy, T., Laszik, Z., Blick, K.E., Johnson, D.L., and Silva, F.G. (1994). Tubular atrophy in the end-stage kidney: a lectin and immunohistochemical study. Hum. Pathol. *25*, 22–28. https://doi.org/10.1016/0046-8177(94)90166-x.

11. Meng, X.M., Nikolic-Paterson, D.J., and Lan, H.Y. (2016). TGF-beta: the master regulator of fibrosis. Nat. Rev. Nephrol. *12*, 325–338. https://doi.org/10.1038/nrneph.2016.48.

12. Humphreys, B.D., Lin, S.L., Kobayashi, A., Hudson, T.E., Nowlin, B.T., Bonventre, J.V., Valerius, M.T., McMahon, A.P., and Duffield, J.S. (2010). Fate tracing reveals the pericyte and not epithelial origin of myofibroblasts in

kidney fibrosis. Am. J. Pathol. *176*, 85–97. https://doi.org/10.2353/ajpath.2010.090517.

13. LeBleu, V.S., Taduri, G., O'Connell, J., Teng, Y., Cooke, V.G., Woda, C., Sugimoto, H., and Kalluri, R. (2013). Origin and function of myofibroblasts in kidney fibrosis. Nat. Med. *19*, 1047–1053. https://doi.org/10.1038/nm.3218.

14. Yang, F., Huang, X.R., Chung, A.C.K., Hou, C.C., Lai, K.N., and Lan, H.Y. (2010). Essential role for Smad3 in angiotensin II-induced tubular epithelial-mesenchymal transition. J. Pathol. *221*, 390–401. https://doi.org/10.1002/path.2721.

15. Kalluri, R., and Weinberg, R.A. (2009). The basics of epithelial-mesenchymal transition. J. Clin. Invest. *119*, 1420–1428. https://doi.org/10.1172/JCI39104.

16. Kriz, W., Kaissling, B., and Le Hir, M. (2011). Epithelial-mesenchymal transition (EMT) in kidney fibrosis: fact or fantasy? J. Clin. Invest. *121*, 468–474. https://doi.org/10.1172/jci44595.

17. Hajarnis, S., Yheskel, M., Williams, D., Brefort, T., Glaudemans, B., Debaix, H., Baum, M., Devuyst, O., and Patel, V. (2018). Suppression of microRNA activity in kidney collecting ducts induces partial loss of epithelial phenotype and renal fibrosis. J. Am. Soc. Nephrol. *29*, 518–531. https://doi.org/10.1681/ASN.2017030334.

18. Grande, M.T., Sánchez-Laorden, B., López-Blau, C., De Frutos, C.A., Boutet, A., Arévalo, M., Rowe, R.G., Weiss, S.J., López-Novoa, J.M., and Nieto, M.A. (2015). Snail1-induced partial epithelial-to-mesenchymal transition drives renal fibrosis in mice and can be targeted to reverse established disease. Nat. Med. *21*, 989–997. https://doi.org/10.1038/nm.3901.

19. Lovisa, S., LeBleu, V.S., Tampe, B., Sugimoto, H., Vadnagara, K., Carstens, J.L., Wu, C.C., Hagos, Y., Burckhardt, B.C., Pentcheva-Hoang, T., et al. (2015). Epithelial-to-mesenchymal transition induces cell cycle arrest and parenchymal damage in renal fibrosis. Nat. Med. *21*, 998–1009. https://doi.org/10.1038/nm.3902.

20. Lovisa, S., Zeisberg, M., and Kalluri, R. (2016). Partial epithelial-to-mesenchymal transition and other new mechanisms of kidney fibrosis. Trends Endocrinol. Metab. *27*, 681–695. https://doi.org/10.1016/j.tem.2016.06.004.

21. Li, L., Zepeda-Orozco, D., Black, R., and Lin, F. (2010). Autophagy is a component of epithelial cell fate in obstructive uropathy. Am. J. Pathol. *176*, 1767–1778. https://doi.org/10.2353/ajpath.2010.090345.

22. Lovisa, S. (2021). Epithelial-to-mesenchymal transition in fibrosis: concepts and targeting strategies. Front. Pharmacol. *12*, 737570. https://doi.org/10.3389/fphar.2021.737570.

23. Borges, F.T., Melo, S.A., Özdemir, B.C., Kato, N., Revuelta, I., Miller, C.A., Gattone, V.H., 2nd, LeBleu, V.S., and Kalluri, R. (2013). TGF-beta1-containing exosomes from injured epithelial cells activate fibroblasts to initiate tissue regenerative responses and fibrosis. J. Am. Soc. Nephrol. *24*, 385–392. https://doi.org/10.1681/ASN.2012101031.

24. Doi, S., Zou, Y., Togao, O., Pastor, J.V., John, G.B., Wang, L., Shiizaki, K., Gotschall, R., Schiavi, S., Yorioka, N., et al. (2011). Klotho inhibits transforming growth factor-beta1 (TGF-beta1) signaling and suppresses renal fibrosis and cancer metastasis in mice. J. Biol. Chem. *286*, 8655–8665. https://doi.org/10.1074/jbc.M110.174037.

25. Grainger, D.J., Kirschenlohr, H.L., Metcalfe, J.C., Weissberg, P.L., Wade, D.P., and Lawn, R.M. (1993). Proliferation of human smooth muscle cells promoted by lipoprotein(a). Science *260*, 1655–1658. https://doi.org/10.1126/science.8503012.

26. Isaka, Y., Brees, D.K., Ikegaya, K., Kaneda, Y., Imai, E., Noble, N.A., and Border, W.A. (1996). Gene therapy by skeletal muscle expression of decorin prevents fibrotic disease in rat kidney. Nat. Med. *2*, 418–423. https://doi.org/10.1038/nm0496-418.

27. Kojima, S., Harpel, P.C., and Rifkin, D.B. (1991). Lipoprotein (a) inhibits the generation of transforming growth factor beta: an endogenous inhibitor of smooth muscle cell migration. J. Cell Biol. *113*, 1439–1445. https://doi.org/10.1083/jcb.113.6.1439.

28. Long, Y.B., Qin, Y.H., Zhou, T.B., and Lei, F.Y. (2012). Association of retinoic acid receptors with extracellular matrix accumulation in rats with renal interstitial fibrosis disease. Int. J. Mol. Sci. *13*, 14073–14085. https://doi.org/10.3390/ijms131114073.

29. Morath, C., Dechow, C., Lehrke, I., Haxsen, V., Waldherr, R., Floege, J., Ritz, E., and Wagner, J. (2001). Effects of retinoids on the TGF-beta system and extracellular matrix in experimental glomerulonephritis. J. Am. Soc. Nephrol. *12*, 2300–2309. https://doi.org/10.1681/ASN.V12112300.

30. Zeisberg, M., Bottiglio, C., Kumar, N., Maeshima, Y., Strutz, F., Müller, G.A., and Kalluri, R. (2003). Bone morphogenic protein-7 inhibits progression of chronic renal fibrosis associated with two genetic mouse models. Am. J. Physiol. Ren. Physiol. *285*, F1060–F1067. https://doi.org/10.1152/ajprenal.00191.2002.

31. Mencke, R., Olauson, H., and Hillebrands, J.L. (2017). Effects of Klotho on fibrosis and cancer: a renal focus on mechanisms and therapeutic strategies. Adv. Drug Deliv. Rev. *121*, 85–100. https://doi.org/10.1016/j.addr.2017.07.009.

32. Yan, Q., Zhu, K., Zhang, L., Fu, Q., Chen, Z., Liu, S., Fu, D., Nakazato, R., Yoshioka, K., Diao, B., et al. (2020). A negative feedback loop between JNK-associated leucine zipper protein and TGF-beta1 regulates kidney fibrosis. Commun. Biol. *3*, 288. https://doi.org/10.1038/s42003-020-1008-z.

33. Dhanasekaran, D.N., Kashef, K., Lee, C.M., Xu, H., and Reddy, E.P. (2007). Scaffold proteins of MAP-kinase modules. Oncogene *26*, 3185–3202. https://doi.org/10.1038/sj.onc.1210411.

34. Wang, H.M., Yan, Q., Yang, T., Cheng, H., Du, J., Yoshioka, K., Kung, S.K.P., and Ding, G.H. (2015). Scaffold protein JLP is critical for CD40 signaling in B lymphocytes. J. Biol. Chem. *290*, 5256–5266. https://doi.org/10.1074/jbc.M114.618496.

35. Ikonomov, O.C., Fligger, J., Sbrissa, D., Dondapati, R., Mlak, K., Deeb, R., and Shisheva, A. (2009). Kinesin adapter JLP links PIKfyve to microtubule-based endosome-to-trans-Golgi network traffic of furin. J. Biol. Chem. *284*, 3750–3761. https://doi.org/10.1074/jbc.M806539200.

36. Verhey, K.J., and Hammond, J.W. (2009). Traffic control: regulation of kinesin motors. Nat. Rev. Mol. Cell Biol. *10*, 765–777. https://doi.org/10.1038/nrm2782.

37. Roberts, A.J., Kon, T., Knight, P.J., Sutoh, K., and Burgess, S.A. (2013). Functions and mechanics of dynein motor proteins. Nat. Rev. Mol. Cell Biol. *14*, 713–726. https://doi.org/10.1038/nrm3667.

38. Wang, H., Zhao, C., Zhang, M., Lee, C.M., Reddy, E.P., and Kung, S.K.P. (2013). A novel role of the scaffolding protein JLP in tuning CD40-induced activation of dendritic cells. Immunobiology *218*, 835–843. https://doi.org/10.1016/j.imbio.2012.10.002.

39. Ha, J.H., Yan, M., Gomathinayagam, R., Jayaraman, M., Husain, S., Liu, J., Mukherjee, P., Reddy, E.P., Song, Y.S., and Dhanasekaran, D.N. (2016). Aberrant expression of JNK-associated leucine-zipper protein, JLP, promotes accelerated growth of ovarian cancer. Oncotarget *7*, 72845–72859. https://doi.org/10.18632/oncotarget.12069.

40. Fu, M.M., and Holzbaur, E.L.F. (2014). Integrated regulation of motor-driven organelle transport by scaffolding proteins. Trends Cell Biol. *24*, 564–574. https://doi.org/10.1016/j.tcb.2014.05.002.

41. Garg, M., Kanojia, D., Suri, S., and Suri, A. (2009). Small interfering RNA-mediated down-regulation of SPAG9 inhibits cervical tumor growth. Cancer *115*, 5688–5699. https://doi.org/10.1002/cncr.24658.

42. Yi, F., Ni, W., Liu, W., Pan, X., Han, X., Yang, L., Kong, X., Ma, R., and Chang, R. (2013). SPAG9 is overexpressed in human astrocytoma and promotes cell proliferation and invasion. Tumour Biol. *34*, 2849–2855. https://doi.org/10.1007/s13277-013-0845-5.

43. Sinha, A., Agarwal, S., Parashar, D., Verma, A., Saini, S., Jagadish, N., Ansari, A.S., Lohiya, N.K., and Suri, A. (2013). Down regulation of SPAG9 reduces growth and invasive potential of triple-negative breast cancer cells: possible implications in targeted therapy. J. Exp. Clin. Cancer Res. *32*, 69. https://doi.org/10.1186/1756-9966-32-69.

44. Li, H., Peng, Y., Niu, H., Wu, B., Zhang, Y., Zhang, Y., Bai, X., and He, P. (2014). SPAG9 is overexpressed in human prostate cancer and promotes cancer cell proliferation. Tumour Biol. *35*, 6949–6954. https://doi.org/10.1007/s13277-014-1947-4.

45. Jiang, J., Liu, Y., Fang, W., and Liu, F. (2014). Sperm-associated antigen 9 promotes

astrocytoma cell invasion through the upregulation of podocalyxin. Mol. Med. Rep. *10*, 417–422. https://doi.org/10.3892/mmr.2014.2168.

46. Chen, F., Lu, Z., Deng, J., Han, X., Bai, J., Liu, Q., Xi, Y., and Zheng, J. (2014). SPAG9 expression is increased in human prostate cancer and promotes cell motility, invasion and angiogenesis in vitro. Oncol. Rep. *32*, 2533–2540. https://doi.org/10.3892/or.2014.3539.

47. Lou, G., Dong, X., Xia, C., Ye, B., Yan, Q., Wu, S., Yu, Y., Liu, F., Zheng, M., Chen, Z., and Liu, Y. (2016). Direct targeting sperm-associated antigen 9 by miR-141 influences hepatocellular carcinoma cell growth and metastasis via JNK pathway. J. Exp. Clin. Cancer Res. *35*, 14. https://doi.org/10.1186/s13046-016-0289-z.

48. Wang, X., Jiang, F., Song, H., Li, X., Xian, J., and Gu, X. (2016). MicroRNA-200a-3p suppresses tumor proliferation and induces apoptosis by targeting SPAG9 in renal cell carcinoma. Biochem. Biophys. Res. Commun. *470*, 620–626. https://doi.org/10.1016/j.bbrc.2016.01.095.

49. Yan, Q., Lou, G., Qian, Y., Qin, B., Xu, X., Wang, Y., Liu, Y., and Dong, X. (2016). SPAG9 is involved in hepatocarcinoma cell migration and invasion via modulation of ELK1 expression. OncoTargets Ther. *9*, 1067–1075. https://doi.org/10.2147/OTT.S98727.

50. Jagadish, N., Gupta, N., Agarwal, S., Parashar, D., Sharma, A., Fatima, R., Topno, A.P., Kumar, V., and Suri, A. (2016). Sperm-associated antigen 9 (SPAG9) promotes the survival and tumor growth of triple-negative breast cancer cells. Tumour Biol. *37*, 13101–13110. https://doi.org/10.1007/s13277-016-5240-6.

51. Li, X., Jiang, F., Wang, X., and Gu, X. (2018). SPAG9 regulates HEF1 expression and drives EMT in bladder transitional cell carcinoma via rac1 signaling pathway. Am. J. Cancer Res. *8*, 2467–2480.

52. Zhang, L., Yan, L., Cao, M., Zhang, H., Li, C., Bai, Y., Yu, P., Li, M., and Zhao, X. (2016). SPAG9 promotes endometrial carcinoma cell invasion through regulation of genes related to the epithelial-mesenchymal transition. Eur. J. Gynaecol. Oncol. *37*, 312–319.

53. Tian, M., Zhang, L., Wang, Y., Deng, M., Peng, C., Liang, W., Ding, G., Shen, B., and Wang, H. (2022). Loss of JNK-associated leucine zipper protein promotes peritoneal dialysis-related peritoneal fibrosis. Kidney Dis. *8*, 168–179. https://doi.org/10.1159/000521564.

54. Noh, M.G., Oh, S.J., Ahn, E.J., Kim, Y.J., Jung, T.Y., Jung, S., Kim, K.K., Lee, J.H., Lee, K.H., and Moon, K.S. (2017). Prognostic significance of E-cadherin and N-cadherin expression in Gliomas. BMC Cancer *17*, 583. https://doi.org/10.1186/s12885-017-3591-z.

55. Zhang, X., Liu, G., Kang, Y., Dong, Z., Qian, Q., and Ma, X. (2013). N-cadherin expression is associated with acquisition of EMT phenotype and with enhanced invasion in erlotinib-resistant lung cancer cell lines. PLoS One *8*, e57692. https://doi.org/10.1371/journal.pone.0057692.

56. Tran, N.L., Nagle, R.B., Cress, A.E., and Heimark, R.L. (1999). N-Cadherin expression in human prostate carcinoma cell lines. An epithelial-mesenchymal transformation mediating adhesion withStromal cells. Am. J. Pathol. *155*, 787–798. https://doi.org/10.1016/S0002-9440(10)65177-2.

57. Eddy, A.A. (2014). Overview of the cellular and molecular basis of kidney fibrosis. Kidney Int. Suppl. *4*, 2–8. https://doi.org/10.1038/kisup.2014.2.

58. Strutz, F., Zeisberg, M., Renziehausen, A., Raschke, B., Becker, V., van Kooten, C., and Müller, G. (2001). TGF-beta 1 induces proliferation in human renal fibroblasts via induction of basic fibroblast growth factor (FGF-2). Kidney Int. *59*, 579–592. https://doi.org/10.1046/j.1523-1755.2001.059002579.x.

59. Akintola, A.D., Crislip, Z.L., Catania, J.M., Chen, G., Zimmer, W.E., Burghardt, R.C., and Parrish, A.R. (2008). Promoter methylation is associated with the age-dependent loss of N-cadherin in the rat kidney. Am. J. Physiol. Renal Physiol. *294*, F170–F176. https://doi.org/10.1152/ajprenal.00285.2007.

60. Peng, Y., Zhang, P., Huang, X., Yan, Q., Wu, M., Xie, R., Wu, Y., Zhang, M., Nan, Q., Zhao, J., et al. (2016). Direct regulation of FOXK1 by C-jun promotes proliferation, invasion and metastasis in gastric cancer cells. Cell Death Dis. *7*, e2480. https://doi.org/10.1038/cddis.2016.225.

61. Chen, F., Xiong, W., Dou, K., and Ran, Q. (2017). Knockdown of FOXK1 suppresses proliferation, migration, and invasion in prostate cancer cells. Oncol. Res. *25*, 1261–1267. https://doi.org/10.3727/096504017X14871164924588.

62. Li, Y., Lv, Z., Zhang, S., Wang, Z., He, L., Tang, M., Pu, W., Zhao, H., Zhang, Z., Shi, Q., et al. (2020). Genetic fate mapping of transient cell fate reveals N-cadherin activity and function in tumor metastasis. Dev. Cell *54*, 593–607.e5. https://doi.org/10.1016/j.devcel.2020.06.021.

63. Beerling, E., Seinstra, D., de Wit, E., Kester, L., van der Velden, D., Maynard, C., Schäfer, R., van Diest, P., Voest, E., van Oudenaarden, A., et al. (2016). Plasticity between epithelial and mesenchymal states unlinks EMT from metastasis-enhancing stem cell capacity. Cell Rep. *14*, 2281–2288. https://doi.org/10.1016/j.celrep.2016.02.034.

64. Pastushenko, I., Brisebarre, A., Sifrim, A., Fioramonti, M., Revenco, T., Boumahdi, S., Van Keymeulen, A., Brown, D., Moers, V., Lemaire, S., et al. (2018). Identification of the tumour transition states occurring during EMT. Nature *556*, 463–468. https://doi.org/10.1038/s41586-018-0040-3.

65. Aiello, N.M., Maddipati, R., Norgard, R.J., Balli, D., Li, J., Yuan, S., Yamazoe, T., Black, T., Sahmoud, A., Furth, E.E., et al. (2018). EMT subtype influences epithelial plasticity and mode of cell migration. Dev. Cell *45*, 681–695.e4. https://doi.org/10.1016/j.devcel.2018.05.027.

66. Kröger, C., Afeyan, A., Mraz, J., Eaton, E.N., Reinhardt, F., Khodor, Y.L., Thiru, P., Bierie, B., Ye, X., Burge, C.B., and Weinberg, R.A. (2019). Acquisition of a hybrid E/M state is essential for tumorigenicity of basal breast cancer cells. Proc. Natl. Acad. Sci. USA *116*, 7353–7362. https://doi.org/10.1073/pnas.1812876116.

67. Saxena, K., Jolly, M.K., and Balamurugan, K. (2020). Hypoxia, partial EMT and collective migration: emerging culprits in metastasis. Transl. Oncol. *13*, 100845. https://doi.org/10.1016/j.tranon.2020.100845.

68. Huang, R.Y.J., Wong, M.K., Tan, T.Z., Kuay, K.T., Ng, A.H.C., Chung, V.Y., Chu, Y.S., Matsumura, N., Lai, H.C., Lee, Y.F., et al. (2013). An EMT spectrum defines an anoikis-resistant and spheroidogenic intermediate mesenchymal state that is sensitive to e-cadherin restoration by a src-kinase inhibitor, saracatinib (AZD0530). Cell Death Dis. *4*, e915. https://doi.org/10.1038/cddis.2013.442.

69. Zhang, J., Tian, X.J., Zhang, H., Teng, Y., Li, R., Bai, F., Elankumaran, S., and Xing, J. (2014). TGF-beta-induced epithelial-to-mesenchymal transition proceeds through stepwise activation of multiple feedback loops. Sci. Signal. *7*, ra91. https://doi.org/10.1126/scisignal.2005304.

70. Hong, T., Watanabe, K., Ta, C.H., Villarreal-Ponce, A., Nie, Q., and Dai, X. (2015). An Ovol2-Zeb1 mutual inhibitory circuit governs bidirectional and multi-step transition between epithelial and mesenchymal states. PLoS Comput. Biol. *11*, e1004569. https://doi.org/10.1371/journal.pcbi.1004569.

71. Jolly, M.K., Tripathi, S.C., Jia, D., Mooney, S.M., Celiktas, M., Hanash, S.M., Mani, S.A., Pienta, K.J., Ben-Jacob, E., and Levine, H. (2016). Stability of the hybrid epithelial/mesenchymal phenotype. Oncotarget *7*, 27067–27084. https://doi.org/10.18632/oncotarget.8166.

72. Bierie, B., Pierce, S.E., Kroeger, C., Stover, D.G., Pattabiraman, D.R., Thiru, P., Liu Donaher, J., Reinhardt, F., Chaffer, C.L., Keckesova, Z., and Weinberg, R.A. (2017). Integrin-beta4 identifies cancer stem cell-enriched populations of partially mesenchymal carcinoma cells. Proc. Natl. Acad. Sci. USA *114*, E2337–E2346. https://doi.org/10.1073/pnas.1618298114.

STAR★METHODS

KEY RESOURCES TABLE

REAGENT or RESOURCE	SOURCE	IDENTIFIER
Antibodies		
JLP	Abcam	Cat#ab12331
Foxk1	Abcam	Cat#ab18196
Foxk1	Santa Cruz	Cat#sc-373810
Fibronectin	Abcam	Cat#ab2413
α-SMA	Abcam	Cat#ab124964
TGF-β1	Abcam	Cat#ab215715
Collagen-I	Abcam	Cat#ab138492
Ki67	Abcam	Cat#ab16667
phospho-histone H3 (pH3)	Abcam	Cat#ab80612
Vimentin	Cell Signaling Technology (CST)	Cat#D21H3
N-cadherin	CST	Cat#13A9
E-cadherin	CST	Cat#24E10
Caspase-3	CST	Cat#5A1E
PARP	CST	Cat#46D11
GAPDH	Proteintech	Cat#60004-1-Ig
Alexa Fluor 488- and 594-conjugated secondary antibodies	Antgene	Cat#Ant024/Ant029
Horseradish peroxidase (HRP)-coupled goat anti-mouse/rabbit IgG	Antgene	Cat#Ant019/Ant020
Bacterial and virus strains		
Jlp shRNA lentivirus	Genechem Co.	N/A
Foxk1 shRNA lentivirus	Genechem Co.	N/A
Cdh2 shRNA lentivirus	Genechem Co.	N/A
pGL3-N-cadherin-Promoter	Biofavor	N/A
pcDNA3.1-Foxk1 plasmid	Biofavor	N/A
pcDNA3.1-JLP-1	Genechem Co.	N/A
Biological samples		
Human kidney tissues from patients with CKD	Renmin hospital of Wuhan University	N/A
Human adjacent normal tissues	Renmin hospital of Wuhan University	N/A
Chemicals, peptides, and recombinant proteins		
Recombinant human TGF-β1	MCE	Cat#HY-P7118
Recombinant human FGF-2	MCE	Cat#HY-P7331
Tamoxifen	Sigma	Cat#T5648
Fetal bovine serum (FBS)	Gibco	Cat#10099-141
DMEM-F12	Hyclone	Cat#SH30023.01
penicillin/streptomycin	Hyclone	Cat#SV30010
DAPI	Sigma	Cat#S7113
Tryptic digestion solution	Beyotime	Cat#C0203
Critical commercial assays		
Annexin V PE Apoptosis Detection Kit	BD	Cat#559763
Cell Cycle Detection Kit	Antgeen	Cat#Ant161

(*Continued on next page*)

Continued		
REAGENT or RESOURCE	SOURCE	IDENTIFIER
Methylated DNA Capture kit	EpiGentek	Cat#P-1034-96
OneStep TUNEL Apoptosis Assay Kit	Beyotime	Cat#C1088
Experimental models: Cell lines		
HK-2 (human kidney 2) cells	ATCC	Cat#CBP60447
Experimental models: Strains		
Ksp1.3-cre mice	Jackson Laboratory	Cat#012237
Oligonucleotides		
Primers for RT-qPCR, see Table S1	This paper	N/A
shRNA sequences for *jlp*: 5′-CCCAGTGTATCAGTCGAGCAA-3′	This paper	N/A
shRNA sequences for *foxk1*: 5′-CUCUCUUUGAACCGUUACUTT-3′	This paper	N/A
shRNA sequences for *cdh2*: 5′-CTGAGCTCAGTTACACTTGAA-3′	This paper	N/A
Software and algorithms		
ImageJ	NIH	https://imagej.nih.gov/ij/
Image Lab	Bio-Rad Laboratories	http://www.bio-rad.com
Wafergen	WaferGen Inc.	http://www.wafergen.com
SmartChip qPCR software	WaferGen Inc.	http://www.wafergen.com
FlowJo	FlowJo, LLC	https://www.flowjo.com/solutions/flowjo/
GraphPad Prism	GraphPad	https://www.graphpad.com/scientific-software/prism/
Other		
Mendeley data for original western blot images	This paper	https://doi.org/10.17632/2f9 rjn74cj.1

RESOURCE AVAILABILITY

Lead contact

Further information and requests for resources and reagents should be directed to and will be fulfilled by the lead contact, Huiming Wang (rm000301@whu.edu.cn).

Materials availability

This study did not generate new unique reagents.

Data and code availability

All data reported in this paper will be shared by the lead contact upon request.

Original western blot images have been deposited at Mendeley and are publicly available as of the date of publication. The DOI is listed in the key resources table.

This study did not generate code.

Additional information required to reanalyze the data reported in this paper is available from the lead contact upon request.

EXPERIMENTAL MODEL AND SUBJECT DETAILS

Mice models

TEC-specific *Jlp*-deficient (Jlp^{cKO}) mice were generated by crossing *Jlp*-floxed mice on a C57BL/6 J background with transgenic mice expressing Cre recombinase under control of the Ksp-cadherin promoter

(*Ksp1.3-cre*) on a C57BL/6 J background. In the *Jlp*-floxed mice, the *loxP* sites were inserted to delete the entire exon 15–18 of the *Jlp* gene, as previously described.[32] *Ksp1.3-cre* mice were purchased from the Jackson Laboratory (Cat# 012237). In order to generate a TEC-specific Jlp transgenic (Tg) mice, the pDONR P2RP3 plasmid, contained a Loxp-STOP-Loxp cassette and a CMV promoter, as well as *mJlp* cDNA domains, was linearized and microinjected into pronuclear-stage zygotes from female C57BL/6N mice, and transferred to pseudo-pregnant females. The established $Cre^{-}Jlp^{TG}$ mice were then mated with Cdh16-Cre-ERT2 knock-in mice, a Cre mouse line which specifically express Cre-ERT2 in the presence of cadherin 16 promoter and were purchased from Cyagen iosciences, Inc., Guangzhou, China. The resulted Cdh16-Cre-ERT2/*mJlp*Tg mice (hereafter as $Cre^{+}Jlp^{TG}$) were given 1.5 mg/day tamoxifen for 6 days (total 9 mg/mouse) at 4–5 weeksold mice by i.p. injection to induce JLP overexpressing with TEC-specific manner. And TEC-specific *cdh2*-deficient mice were bred in a similar way as Jlp^{cKO} mice.

TEC-specific *Jlp*-knockout mice and the corresponding control mice with wild-type JLP expression ($Jlp^{flox/flox}$) and TEC-specific JLP transgenic ($Cre^{+}Jlp^{TG}$) mice and the corresponding control mice with wild-type JLP expression ($Cre^{-}Jlp^{TG}$). The resulting mice with the genotype of Ksp-Cre^{+}/$cdh2^{loxP/loxP}$ were confirmed to be TEC-specific *cdh2* defective and referred to as $cdh2^{cKO}$ mice (Figures 6A and 6B).

The mouse models used in this study were created using 8–10-week-old male and female mice weighing 20–30 g. The UUO mouse model was established as previously described.[32] The indicated mice were subjected to treatment to generate IRI-induced kidney fibrosis. Mice were anesthetized and the left kidney was exposed, then the renal pedicle was clamped using a microvessel clip at 37°C for 30 min. A sham operation for UUO or IRI was performed in the contralateral kidney. The mice were sacrificed on the indicated days, and the kidneys were collected for subsequent experiments. The mice were reared under specific pathogen-free conditions at the Center for Animal Experiments of Wuhan University. All animal experiments were approved by the Animal Ethics Review Board of Wuhan University (Approval No. WDRM-20211102). and performed according to the guidelines of the National Health and Medical Research Council of China.

Human biopsy specimens

Human renal biopsy specimens were obtained from patients with normal or chronic impaired renal function (CKD). The clinical ethics committee approved the human study of the Renmin Hospital of Wuhan University (WDRY2021-KS045), and all patients provided informed consent before inclusion in this study.

Cell culture and treatment

The human proximal tubular epithelial cells (HK-2) were purchased from the AmericanType Culture Collection (ATCC). Cells were cultured in DMEM-F12 medium supplemented with 10% FBS and 1% penicillin/streptomycin at 37°C and 5% CO_2. The cells were incubated with or without 10 ng/mL of TGF-β1 or FGF-2 for the indicated times. Cell transfection was performed according to the manufacturer's instructions. Briefly, 2×10^5 cells were transfected with lentiviral vectors (Genechem Co., Shanghai, China) for stable shRNA with the indicated gene or scrambled gene target using a lentivirus infection reagent (Genechem Co) for 16 h in 6-well plates. Puromycin was used to screen for stably infected cells. Under some conditions, plasmid constructs encoding human *Jlp* (pcDNA3.1-JLP-1, from Genechem Co) or a mock gene were transfected into HK-2 cells using Lipofectamine® 8000 (Beyotime, Nantong, China) to generate *jlp*-overexpressing (referred to as jlp^{OE}) cells or wild-type JLP-expressing control cells (jlp^{Ctrl}).

METHOD DETAILS

Histopathology and immunohistochemistry

Kidney samples were fixed in 4% paraformaldehyde and embedded in paraffin. Tissue sections (4 μm) were stained with HE and Masson staining according to the manufacturer's protocols for histological microscopic examination. Slides were observed under an Olympus microscope (Olympus, Tokyo, Japan). The visual fields (×200 magnification) from five individual experiments were randomly selected. HE staining was performed using standard procedures.- Tubular injury was assessed by grading tubular dilatation, epithelial simplification and brush border loss in ten randomly chosen, non-overlapping fields (×400 magnification). For immunohistochemical staining, sections were first deparaffinized, hydrated, antigen repaired, and incubated with the indicated primary antibodies. Five fields (×200 magnification) from

individual groups were randomly selected, and the percentage of the positively stained area was quantified using ImageJ ver. 1.37c analysis software (NIH, Bethesda, MD, USA).

Immunofluorescence staining

For immunofluorescence (IF) staining, kidney tissue sections were deparaffinized, hydrated, antigen repaired, blocked, then incubated with the indicated primary antibodies. Or cultured cells were fixed (4% paraformaldehyde) and blocked, then incubated with the indicated primary antibodies. Primary antibodies against JLP, TGF-β1, FN, α-SMA, vimentin, N-cadherin, Ki67, and pH3, and secondary antibodies conjugated with Alexa Fluor 488, 594, or 647-conjugation were used. The samples were stained with DAPI and ProLong Gold (Life Technologies, Carlsbad, CA, USA). Slides were visualized using a confocal laser microscope (FV1200; Olympus). Five visual fields (×1000 magnification) of each group from three individual experiments were randomly selected, and the fluorescence intensity of IF staining was quantified using ImageJ analysis software. Under some conditions, tissue sections were subjected to apoptosis detection using the OneStep TUNEL Apoptosis Assay Kit (Beyotime) according to the manufacturer's instructions.

Western blotting

Western blotting was performed using standard methods. Briefly, harvested kidney cortex tissues or cultured HK-2 cells were lysed in RIPA buffer with protease inhibitor cocktail on ice for 30 min. Protein levels were quantified using Bradford method. Lysed samples were loaded onto 8% or 12% SDS gels for electrophoresis and transferred onto PVDF membranes (MilliporeSigma, Burlington, MA, USA) using the X-cell SureLock Mini-Cell system (Invitrogen, Thermo Fisher Scientific). PVDF membranes were then blocked in 5% skim milk at room temperature (20–24°C) for 1 h and incubated with the indicated primary antibodies at 4°C overnight. Membranes were incubated with HRP secondary antibodies. Blots were chemiluminescence using enhanced chemiluminescence (ECL) luminous fluid and ChemiDoc XR Plus (Bio-Rad Laboratories, Hercules, CA, USA). Quantity One analysis software (Bio-Rad Laboratories) was used to quantify the band intensity of some proteins; at least three bands from three individual experiments were used for band intensity analysis.

Quantitative real-time PCR (qRT-PCR)

Total RNA was extracted from kidney cortical tissues or HK-2 cells using TRIzol reagent (Invitrogen). cDNA was synthesized using the RevertAid cDNA Synthesis Kit (Thermo Fisher Scientific). qPCR was performed using an ABI7900 RT-PCR system (Illumina, San Diego, CA, USA) with SYBR Green PCR Master Mix according to the manufacturer's instructions. Gene expression measurements were standardized to that of the *gapdh* housekeeping gene. Relative gene expression was calculated using the comparative CT method ($2^{-\Delta\Delta}$CT) with the control group normalized to a fold value of 1. The primer pair sequences used in this study are listed in Table S1.

Cell migration assay

HK-2 cells were cultured in 6-well plates, scratched with a 1 mL sterile pipette tip, then washed with PBS, and incubated in a serum-free medium at 37°C. Gaps in wound healing were recorded from 0 to 48 h using an inverted phase-contrast microscope. A quantitative comparison of the number of cells crossing the threshold in the wounded regions was made.

Methylated DNA immunoprecipitation (MeDIP) assay

DNA was extracted from kidney tissue and sheared ultrasonically. The sonicated DNA was then processed using the Methylated DNA Capture kit (EpiGentek, Farmingdale, NY, USA) to enrich methylated fragments according to the manufacturer's instructions. The immunoprecipitated fragments were harvested and subjected to real-time qPCR (PCR master mix, arraystar) under the following conditions: denaturation and enzyme activation at 95°C for 10 min, amplification for 40 PCR-cycles at 95°C for 10 s, followed by annealing at 60°C for 60 s. The melting process was automatically generated using Wafergen software. The qPCR results were analyzed using SmartChip qPCR software.

Luciferase reporter assay

The human N-cadherin gene promoter region was inserted into a pGL3 basic vector as pGL3-N-cadherin-Promoter (Biofavor, Wuhan, China). One hundred nanograms of the constructed plasmid and seven nanograms of renilla luciferase control plasmid were transfected into HEK293T cells expressing Foxk1 cDNA,

which had previously been transfected with a pcDNA3.1-Foxk1 plasmid (Biofavor) in six-well plates. Luciferase activity was measured after 24 h using a Dual Luciferase Assay Kit (Promega, Madison, WI, USA). Renilla luciferase was used to normalize the reporter luciferase activity. Each transfection was performed in triplicate.

Flow cytometric analysis

Cell apoptosis and cycle assays were performed using the PE Annexin V Apoptosis Detection Kit (BD Biosciences, Franklin Lakes, NJ, USA) and Cell Cycle Detection Kit (Antgeen) according to the manufacturer's instructions. Briefly, cells were collected and stained with PE Annexin V and 7-AAD for 15 min in the dark and then subjected to flow cytometry. For cell cycle assay, cells were collected and fixed for 4 hat 4°C in 75% pre-chilled ethanol, followed by resuspension with 150 μL of RNAase and 150 μL of propidium iodide (PI) stepwise. The harvested cell samples were subjected to flow cytometry. All data were processed using the FlowJo software (v 10.6.2).

QUANTIFICATION AND STATISTICAL ANALYSIS

Quantitative data are presented as the mean ± SEM. Statistical analyses were conducted using SPSS version 20.0, and the GraphPad Prism 8 software package. Statistical comparison of the groups was performed using one-way analysis of variance, and the least significant difference test was used for multiple comparisons. Statistical significance was set as $p < 0.05$.